TESS

Transiting Exoplanet Survey Satellite

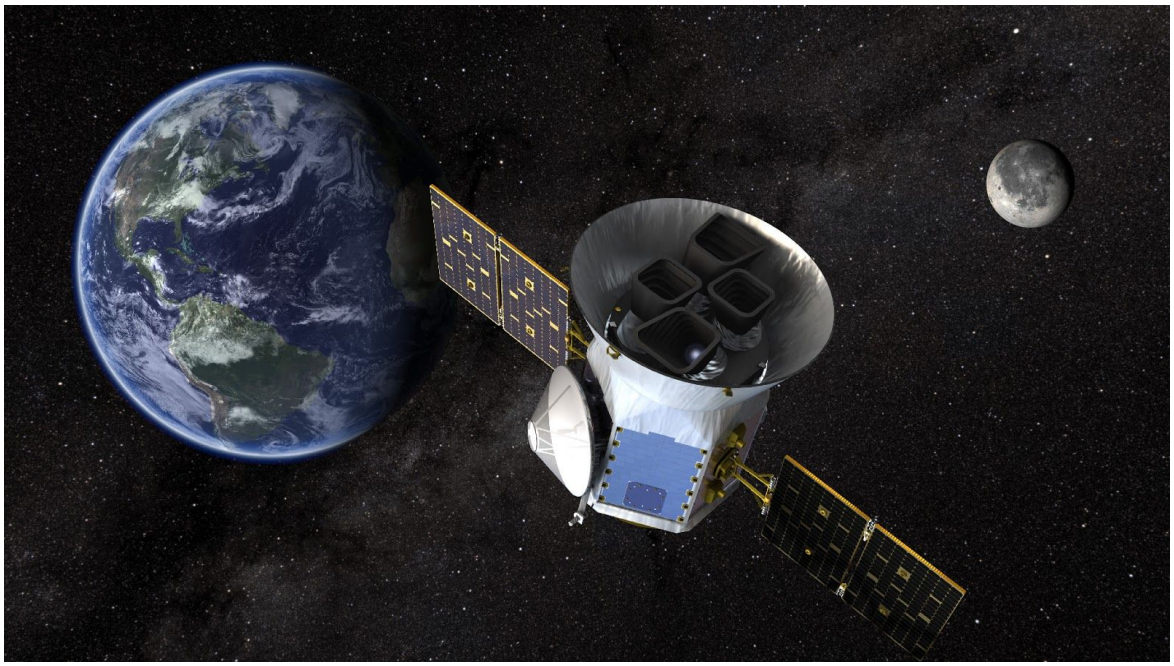

Credit: NASA

Critical Design Review

Under the guidance of Professor Stephen Robinson,

Michael Gonzales
Bobby Hodgson
Abhinav Kamath
Evan Lange
Inbal Shlesinger

CDR OUTLINE

1. Introduction

1.1 Vehicle Overview: Purpose, Timescale, and Overall Specifications

The purpose of the Transiting Exoplanet Survey Satellite, or TESS, is to find exoplanets and to gather information, such as planet volume and atmospheric composition.

TESS was announced for launch on April 5, 2013 and was actually launched on April 18, 2018 from Cape Canaveral Air Force Station aboard a SpaceX Falcon 9 rocket. TESS began science operations on July 25, 2018 and the total mission time is 2 years. After the mission ends, it is capable of remaining in orbit for decades so there is no known plan for deorbit at this time.

TESS stands at 1.5 m tall and 1.2 m wide (3.7 m with the solar panels extended). The solar panels are 0.89 m tall. See Figure 1.1.1 below for an illustration of the size specifications of TESS. The launch mass is 362 kg.

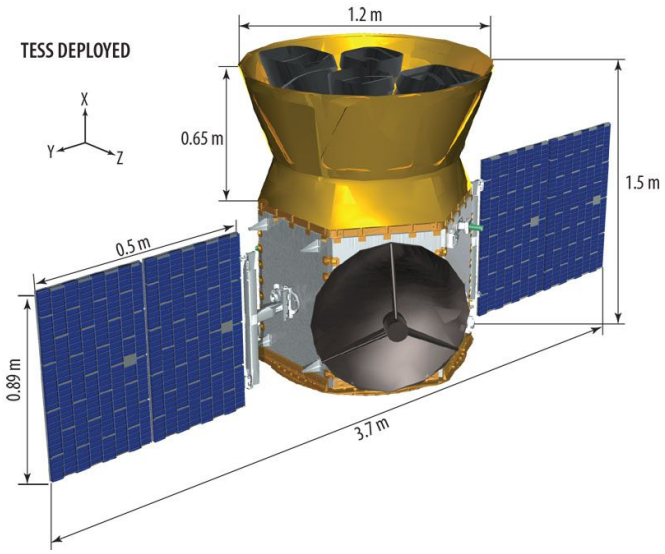

Figure 1.1.1: TESS Size Specifications (*Credit: Spaceflight 101*)

1.2 Customers and Stakeholder Requirements

1.2.1 Customers and Other Stakeholders

The stakeholders for the TESS mission are from a diverse group of government, educational, and private companies. Leading this endeavor and defining the mission objectives is the Massachusetts Institute of Technology (MIT). They developed the camera payload for TESS and operate the TESS Science Office to collect and analyze data from the satellite.

Carrying the MIT camera payload is done by the LEOStar-2/750 Spacecraft bus designed by Northrop Grumman. Their spacecraft must be reliable to carry out TESS mission objectives.

Launching TESS into mission orbit is provided by SpaceX and their Falcon 9 Rocket. They must ensure that their rocket will survive launch in order to deploy TESS to the mission orbit.

Operations of TESS after launch is carried out by the Orbital Sciences Corporation. They are in charge of the day-to-day operations of TESS to carry out the mission objectives.

Project management is provided by the venerable National Aeronautics and Space Administration (NASA). Their experience in space mission success and failure is invaluable to overall coordination between MIT, Northrop Grumman, SpaceX, and Orbital Sciences Corporation. NASA also provides the launch facilities for Falcon 9 rocket, systems engineering experience for safety and mission assurance.

Supplementary stakeholders are the people and organizations that benefit from the success of the TESS mission. Assisting with the TESS Science Office is the Harvard Smithsonian Center For Astrophysics (CFA). They provide analyses of the data results from TESS mission in conjunction with MIT. Taxpayers in the US provide the funding to Congress who allocates funding to NASA to carry out space missions.

1.2.2 Benefits and Stakes

Being a leader in exoplanet discovery and research is the primary motivation for MIT. Failure could divert research funding to other universities.

Success for Northrop Grumman in the TESS mission will provide valuable data in the performance of the LEOStar-2/750 Spacecraft design. Failure would push future clients to other spacecraft manufacturers and force a redesign process to stay relevant in future space missions.

SpaceX would benefit in a successful mission since it allows them to prove the reliability of the Falcon 9 and their first stage recovery operations in future space missions. Failure can risk future space contracts with NASA and other organizations.

Operational success will build experience for Orbital Sciences Corporation as a premiere spacecraft operator for future space missions. Failure would reduce trust in their ability to operate future spacecraft.

A success for NASA ensures continued public support for future space missions. Failure risks a skeptical Congress from allocating future funding for space missions.

Successful imaging data from TESS for the CFA provides mutual benefit to MIT in exoplanet research. Failure means a lost opportunity to learn more about exoplanets.

Public opinion will improve US Taxpayer public opinion of NASA upon a successful TESS mission. Failure decreases public support for future space missions.

1.3 Mission Objectives

TESS' mission objectives are to survey 200,000 of the brightest stars near the sun and to search for transiting exoplanets and ecliptic binary stars. Although the purpose of the Kepler telescope was also to survey the sky, TESS covers 400 times the area Kepler did.

TESS uses the amount of starlight absorbed by these planets' atmospheres, which could allow us to make spectroscopic observations that can give us insight into the

planets' atmospheric conditions. When observing the exoplanets, TESS is looking for atmospheric condition and structure, transmission and emission spectrum data, albedo, phase function, clouds, and winds. TESS scans stellar spectral types F5 to M5.

TESS can also provide us with size measurements of the planets, which could be used to find their volumes. The volumes, combined with the known masses of these planets allows us to calculate the planet densities.

1.4 Concept of Operations

TESS was launched on a SpaceX Falcon 9 rocket from Cape Canaveral Air Force Station. After launch, TESS follows a concept of operations that ends in a unique orbit.

TESS is sent into an initial 600 km parking orbit with an orbital inclination of 28.5 degrees. Once in this orbit, the lower adapter structure is released from the solid rocket motor and the stack spin rate is increased to 60 rpm. As the solid rocket motor burns out, it is released and falls away. After they separate, TESS uses hydrazine thrusters to despin and then transitions into its first phase orbit with an apogee of approximately 250,000 km. At the perigee of this phasing orbit, TESS performs a burn to increase the apogee to approximately 325,000 km and then repeats this to increase the apogee one more time to approximately 400,000 km. This puts TESS very close to the moon. At this point, TESS uses lunar gravity assist to get to the final orbit, which has an orbital inclination of 37 degrees and puts TESS in a 2:1 lunar resonance.

Once in its final orbit, TESS can begin its 2 year mission. TESS transitions between HASO (high-altitude science operations) in which it collects data and LAHO (low-altitude housekeeping operations) in which it points its Ka-Band high gain antenna towards one of the three deep space network stations and downlinks information, which takes a total of 16 hours (12 to orient and 4 to downlink data).

Once in this final orbit, TESS uses the moon's gravity to stabilize its orbit and stay in its final orbit for decades with very little adjustment required from the thrusters.

See Figures 1.4.1 through 1.4.3 below for illustrations of the concept of operations and TESS' maneuvers.

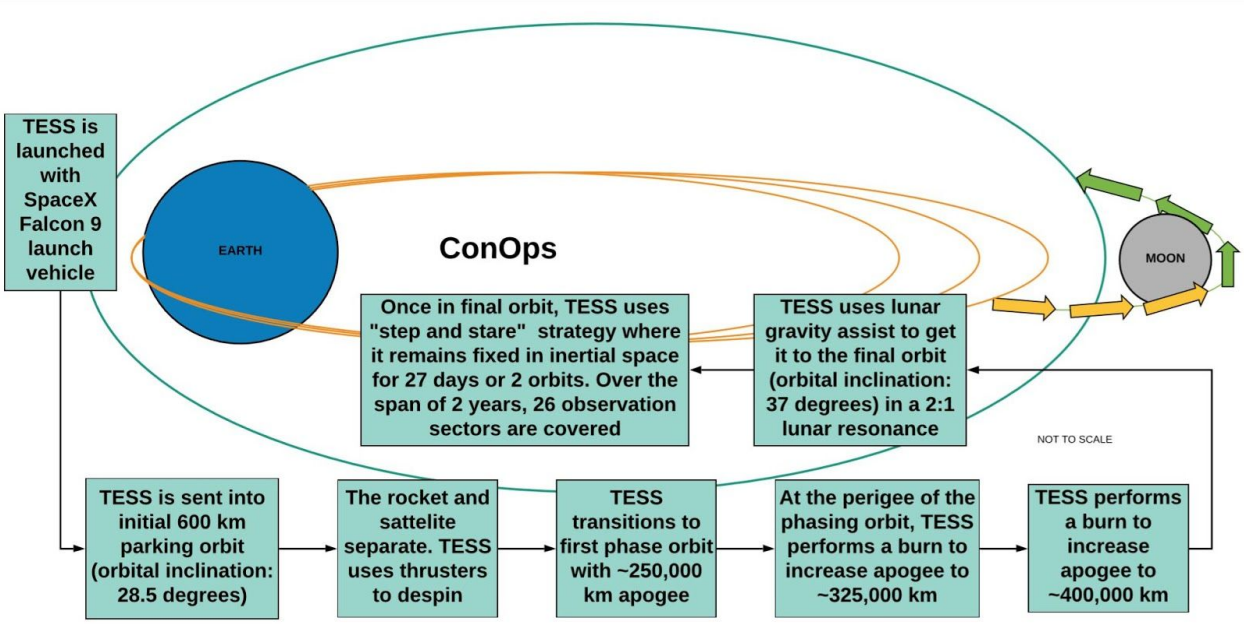

Figure 1.4.1: TESS Concept of Operations Diagram

Figure 1.4.2: Northern Hemisphere of Viewing Sectors

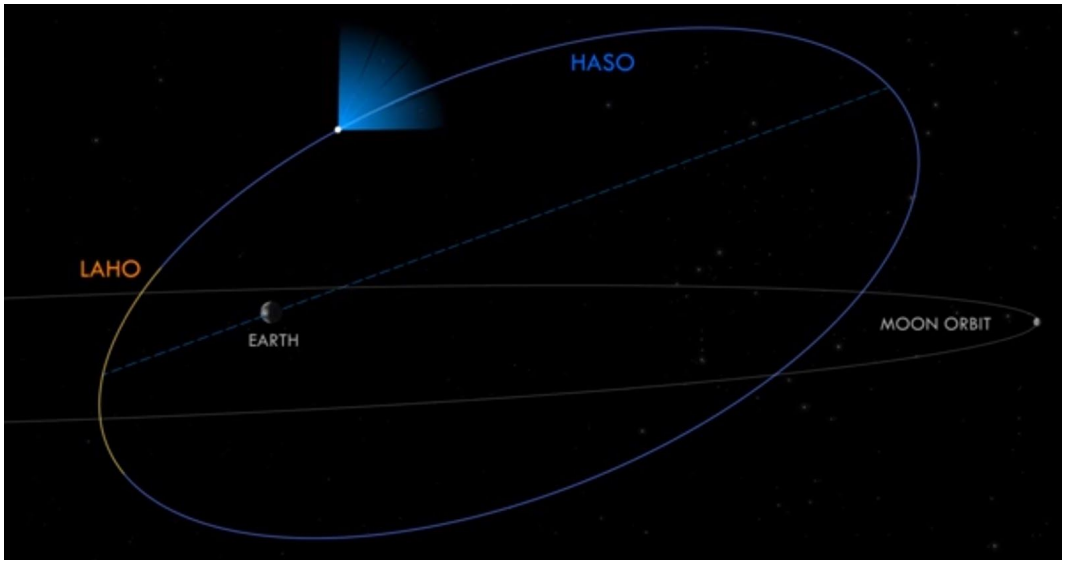

Figure 1.4.3: Areas of HASO and LAHO

1.5 Product Breakdown Structure

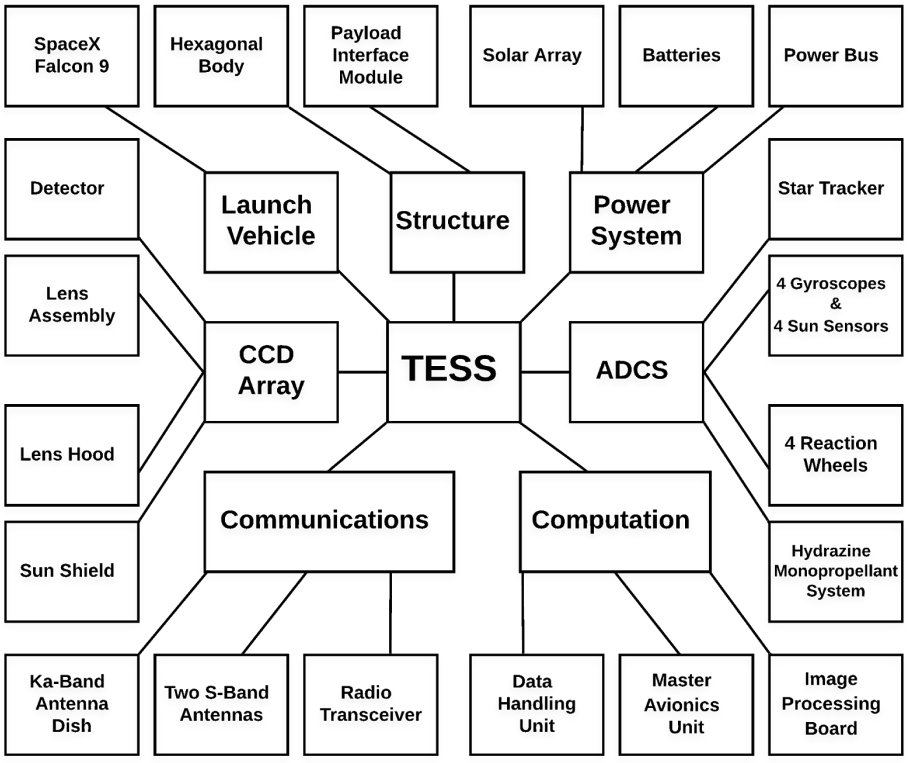

Figure 1.5.1: TESS Product Breakdown Diagram

1.5.1 Launch Vehicle

Launch Vehicle: TESS was launched into LEO by a SpaceX Falcon 9 Rocket. The first stage is comprised of nine Merlin Engines and the second stage is one Merlin 1D Engine.

1.5.2 Structure

The satellite bus is a variant of the LEOStar-2/750, designed by Northrop Grumman. This spacecraft bus has proven itself to be reliable across six different missions before TESS. The mass of the satellite is 362 kg.

1.5.3 Power System

To power the other systems onboard and carry out the mission objectives, two Solar Arrays capable of providing 530 watts end of life (EoL) performance to the power bus. End of life performance refers to the ability of the solar arry to work at the end of the service life. These solar arrays, measuring 1.1 meters by 0.89 meters each, are capable of both fixed and articulating modes. The power bus converts the voltage generated by the solar panels down to a stable 28 volts for charging the Satellite's batteries and supplying the rest of the satellite with power.

1.5.4 Attitude Determination Control System

During science operations, the CCD array acts as a star tracker by referencing the centroids of 200 photometric guide stars. During non-science operations, a dual-redundant μASC Star Tracker by DTU Space is used to provide the satellite with an attitude accurate to 2 arcseconds. The inertia tensor of the satellite is measured using four gyroscopes. Four sun sensors provide a solar vector at the lens hood of each camera to measure any interference generated by the sun. The attitude is altered using four reaction wheels made by Honeywell, capable of an accuracy of 3.6 arcseconds and a stability of 0.05 arcseconds per hour. The reaction wheels are desaturated using four 5 N hydrazine thrusters. A 22 N hydrazine thruster is used for a Prograde burn into the final orbit. A 45 kg propellant tank provides the thrusters with enough fuel for a delta-V of 268m/s.

1.5.5 Computation

Image processing and attitude determination is completed by the Data Handling Unit (DHU). Which is comprised of a SEAKR Athena-3 and Virtex-5 FPGA. The attitudes are sent to the Master Avionics Unit (MAU). The MAU converts these attitudes into the necessary attitude adjustments and controls the reaction wheels accordingly.

1.5.6 Communications

During Downlink, a 0.7m parabolic Ka-Band antenna dish is used to communicate with NASA's Deep Space Network (DSN) at the maximum 100 Mb/s. Two omni-directional S-Band antennas are used for long distance communication.

1.5.7 Charged-Coupled Device Array

The CCD Array is made up of four cameras, each with a field of view (FOV) of 24 by 24 degrees. Each camera has a detector made up of 4096x4096 pixels. The Lens assembly has an f -number of 1.4 and reduces spherical aberrations. The lens hood protects the detectors from sunlight and passively cools them down to the optimal temperature.

2. Background

2.1 History

2.1.1 Previous Spacecraft Designs

Finding exoplanets with spacecraft started with the Hubble Space Telescope, Spitzer, and Kepler as seen in Figure 2.1.1 [1].

Ground-based observatories all around the surface of the Earth have been used to observe the radio and visible light sections of the electromagnetic spectrum. Some notable examples include the Fred Lawrence Whipple Observatory and the Very Energetic Radiation Imaging Telescope Array System, both in Arizona [29].

According to NASA Official Dunbar in *The Hubble Story*, The Hubble Space Telescope was a large visible spectrum space telescope delivered to orbit April 4, 1990 by the Space Shuttle Discovery [2]. The Hubble Space Telescope has a pointing accuracy of seven thousandths of an arcsecond allowing it to image very distant stars. During its service life, according to Dunbar's *About the Hubble Space Telescope*, it transmits 150 gigabits per week of imaging data. Shortly after launch Hubble was noted for having a mirror defect due to a manufacturing defect resulting in a service mission to add corrective lenses [9].

Next in line, according to Jet Propulsion Laboratory's *Fast Facts*, was the Spitzer Infrared Space Telescope that was launched August 25, 2003 onboard a Delta 7920H ELV rocket [4]. Spitzer has a cold mission time of two and a half years, due to needing cryogenic cooling for the infrared sensor. The ACS of Spitzer is capable of tracking up to 1 arcsecond.

Similarly, Kepler was launched on a Delta D2925-10L rocket [5]. According to NASA, the Kepler mission discovered 2,600 exoplanets in the Cygnus-Lyra region of space [6]. During the mission one of its reaction wheels failed during July of 2012 and less than a year later (May 2013) another reaction wheel failed forcing, thus disabling the ACS [10]. Kepler was retired in October 30th, 2018 after running out of fuel to continue observations.

The James Webb Space Telescope will be used to observe all parts of history in time and space from the Big Bang to the evolution of our Solar System. The telescope is capable of detecting very faint signals and will be very useful in helping map out the sky [30].

The Wide Field Infrared Survey Telescope (WFIRST) will perform wide field imaging of the infrared sky. It is about the size of the Hubble Space Telescope and will cover a field of view 100 times larger than the Hubble [31].

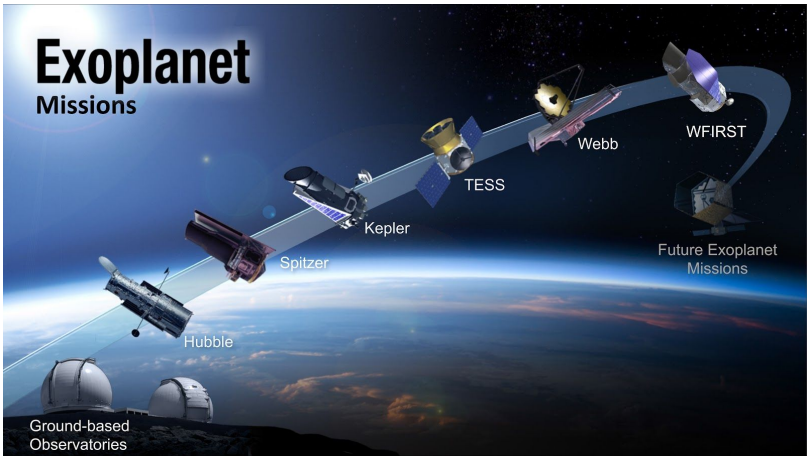

Figure 2.1.1: Graphic of Exoplanet Missions from past to future (*Credit: NASA*).

2.2 Literature

2.2.1 Features of TESS that Improve upon Previous Missions

TESS is based on a LEOStar-2/750 Spacecraft designed and built by Northrop Grumman with a total launch mass of 362 kg, which has a lighter launch mass than the 950 kg Spitzer and the 10,886 kg Hubble Space Telescope [1, 7]. According to the *TESS Science Writer's Guide*, TESS improves upon Kepler and K2 missions by covering 85% of the sky as seen in Figure 2.2.1 [8]. The additional area covered is about 400 times larger than covered by Kepler. Additionally, TESS scans 26 sectors of the sky, as seen in Figure 2.2.2, in order to find exoplanets for the future James Webb Space Telescope mission in the 2020s. In terms of ACS accuracy, TESS can point with 3.6 arcseconds. The High Earth Orbit (HEO) is very stable and unobstructed by the Earth or Moon during its observations. The HEO orbit also allows for potential observation missions after the initial 2-year main mission. Furthermore, its 2:1 orbital resonance with the Moon allows TESS to pass closer to Earth to transmit its observation data.

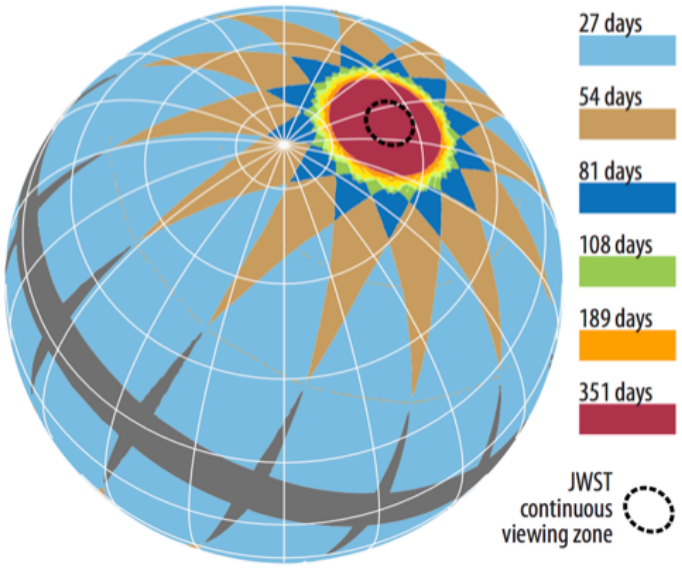

Figure 2.2.1: TESS coverage area during 2-year mission. The grey band was covered by the Hubble Space Telescope and Kepler missions (*Credit: NASA*).

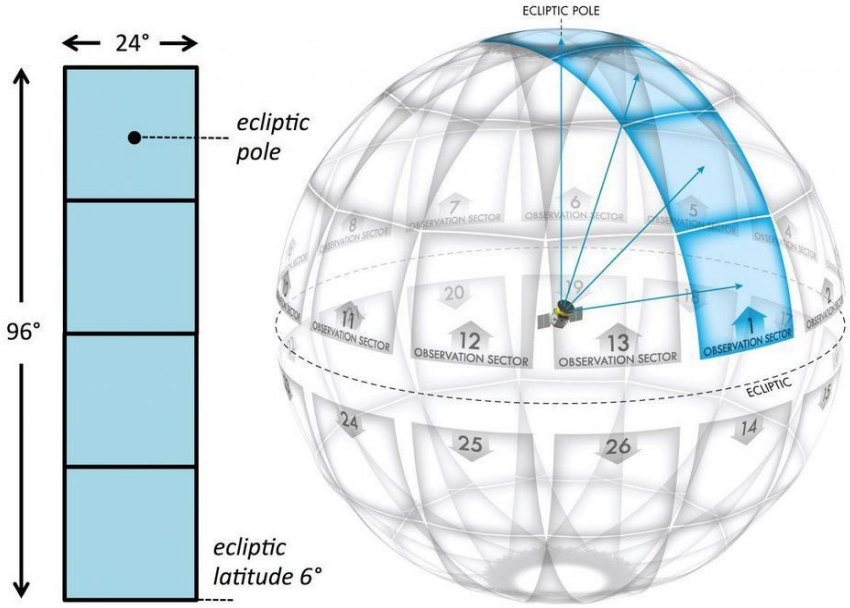

Figure 2.2.2: TESS divides the sky into 26 observation sectors (13 per celestial hemisphere) each spanning 24 by 96 degrees. TESS will spend its first year surveying the southern sky, then begin the northern survey. (*Credit: medium.com*)

3. Design to Meet Mission Requirements

3.1 Full Subsystem Overview and Breakdown

TESS is comprised of numerous systems. These subsystems are organized as levels that flow down from level 1, which is the spacecraft in its entirety.

3.1.1 Intro to the Level 1 System

The Level 1 system is the spacecraft, TESS.

3.1.2 Level 2: Main Subsystems

Level 2 consists of 7 main systems. First, is the launch vehicle system which allows TESS to be sent into its mission orbit. Second, is the structure system which supports the initial launch loads, such as maximum dynamic pressure and carry all of the other systems onboard the LeoStar 2 bus. Third is the power system that provides power to the remaining systems so that the mission requirements can be met. Next is the attitude control system, ADCS, which has the responsibility of pointing TESS in the correct directions during the various orbital burns as well as point the observatory in the correct direction in the mission observation sectors. Fifth, is the computation system onboard TESS which is tasked with sorting the data inputs from the other systems and then sends mission related commands to permanent subsystems in order to carry out the mission requirements. Sixth, is the communications system. This subsystem sends system information and imaging data to the ground station as well as receives commands from the ground station for reorientation and other such operations. Seventh, is the CCD array system is the mission critical camera, optical telescope, payload tasked with capturing images of stars in each mission observation sector for later downlink to the ground station.

3.1.3 Level 3: Level 2 Subsystems

Level 3 further dives into the specifics by dividing the level 2 subsystems into even more systems.

The launch vehicle of level 2 is the SpaceX Falcon 9 Rocket which consists of a reusable 1st stage that includes 9 Merlin rocket engines, a 2nd stage using a single

Merlin rocket engine, and a payload section capable of fitting TESS. The payload interface module subsystem allows TESS to be loaded onto the Falcon 9 Rocket.

The LEOStar 2 bus serves as the primary structure subsystem for TESS and supports the mission payload and other subsystems with a combined launch mass of 362 kg [16].

The solar array, batteries, and power bus are the three subsystems of the power system. The solar array gathers sunlight and converts it into electrical energy that is stored into batteries as chemical energy through the power bus. The power bus regulates the incoming power from the solar panels into a steady state flow of current to charge the batteries. For other subsystems, the power bus can adjust the output voltage to meet the subsystem demands of up to 28 V. The average power provided during typical mission operations is 415 W [15].

The ACS system is comprised of four subsystems. The star tracker consists of a camera connected to the onboard computer to compare observed stars to known constellations and thus determine the current attitude of the satellite. For redundancy, attitude determination a set of four gyroscopes and four sun sensors are used. The gyroscopes are placed on reaction wheels to determine orientation relative to the axis of spin. Sun sensors are passive elements, devices that don't require power to use, that determine where the Sun is in reference to TESS in order to avoid pointing the camera payload at the Sun [17]. Four Honeywell made custom reaction wheels are used to control the attitude of TESS. These reaction wheels are rated to 9000 revolutions per minute and are capable of pointing TESS with an accuracy of 3.2 arcseconds with stability of 0.05 arcseconds per hour [15]. Station keeping, rough slewing maneuvers, and offloading momentum from the reaction wheels are done by the hydrazine monopropellant system. The launch weight of the hydrazine fuel is 45 kg [15]

The computation system is comprised of three subsystems. The first is the image processing board that takes the image data and converts them to a readable file format for downlink. The ACS system is controlled by the master avionics unit. Lastly, the data handling unit passes data to and from each subsystem and stores data for downlink.

The CCD array consists of the sun shield to protect the CCD light detector against direct sunlight exposure. The lens hood reduces the glare from stars outside the observation sector, especially the Sun. The lens assembly focuses the light onto the CCD detector so it can capture light and convert it into an image.

3.1.4 Level 4: Level 3 Subsystems to Meet Mission Requirements

Level 4 consists of the quantitative requirements for each level 3 subsystem in order to accomplish the mission requirements. The Falcon 9 launch vehicle must deliver TESS into mission orbit safely. The LEOStar-2 bus structure must be able to survive launch conditions as well as the space environment. The power cannot exceed the end-of-life solar power generation limit of 530 W. The reaction wheels must maintain a minimum accuracy of 3.5 arcseconds and have a stability of 0.05 arcseconds per hour. The primary hydrazine orbital maneuvering thruster has a thrust output of 22 N is used for orbital corrections and station keeping. Four attitude control thrusters capable of 5 N of thrust are used for slewing and desaturating the reaction wheels. The primary mission is designed for a delta V of 215 m/s. The max delta V budget is 268 m/s. The computation subsystems mustn't exceed the storage memory of 192 GB of flash memory. The communication subsystems needs to remain below 4 W in transmitting or receiving data. The CCD array subsystems must image the mission observation sectors.

3.2 Modification Subsystems: Antenna Positioning Mechanism

The antenna positioning mechanism modification modifies the structure subsystem, the power subsystem, and the ACS subsystems. The mechanism is being added to the structure. The power system is modified due to the added power necessary to operate the gimbal at the end of the deployable mast. The ACS is changed because the addition of this mast will require different torques to correct for the added inertia on the entire satellite.

3.2.1 Reasoning for Antenna Modification Choice

In order to maximize the area viewed by TESS' cameras, we want to "stitch" together the observation sectors more tightly and add an extra observation sector to each hemisphere, thus increasing the total number of observation sectors from 26 to 28. We plan on doing this by simultaneously downlinking data and performing scientific operations during the original downlink window, during which TESS, at present, halts scientific operations in order to orient towards the Deep Space Networks on Earth and downlink information. If we could simultaneously gather data while downlinking, we would increase the time TESS spends on scientific operations by 16 hours for every

orbit. For a 13.7-day orbit and a two-year mission, this would add enough time to include an extra observation sector to each hemisphere, increasing the total sky coverage from 85.00% to 86.65%, and considering the fact that the “equatorial belt” was intentionally excluded from observation, TESS would now be able to cover 96.78% of the portion of sky under consideration, as opposed to 94.94% (1.84% increase in coverage).

In order to be able to gather data while downlinking, we propose to mount TESS’ high-gain Ka-band antenna on a 2DOF gimbal and project it by means of a deployable mast. This will allow for the antenna to track the Earth, without needing to reorient the entire satellite.

Our design for the antenna positioning mechanism was based on the JPL NuSTAR telescope, shown in Figure 3.2.1a and the Shuttle Radar Topography Mission (SRTM), shown in Figure 3.2.1b.

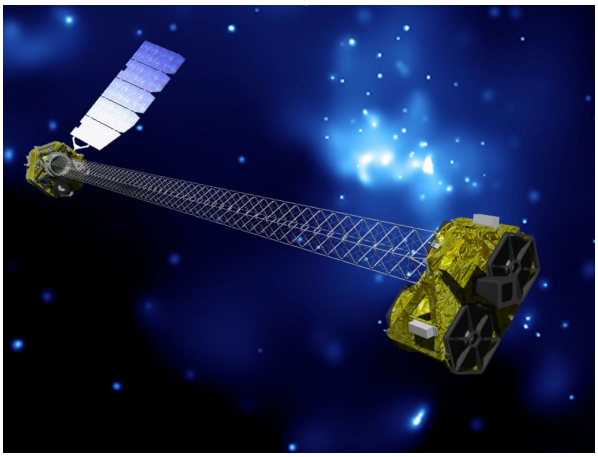

Figure 3.2.1a: JPL NuSTAR Telescope with Extension Mast (*Credit: NASA*)

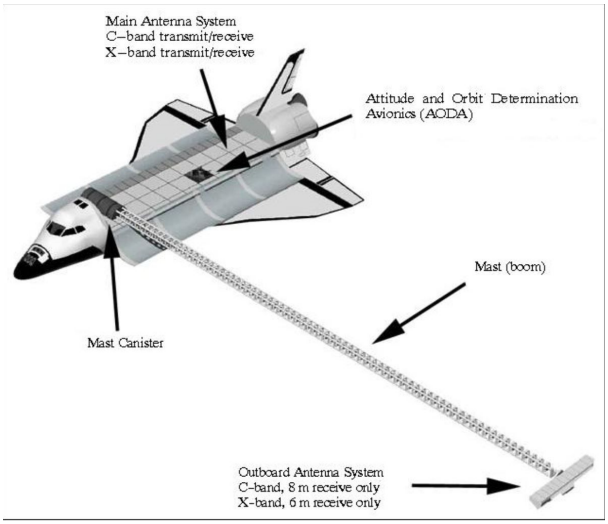

Figure 3.2.1b: SRTM with Extension Mast (*Credit: eoPortal Sharing Earth Observation Resources Directory*)

3.2.2 Requirements for Antenna Modification

One important requirement for adding an antenna positioning mechanism to the satellite is to make sure it remains a zero-momentum system. The mass and length of the mast have to be taken into account when designing the ACS system because the movement of an extended body will impart a torque on the entire body, which must be corrected in order to keep TESS from rotating when the antenna moves.

Another major requirement for the mast is making sure it's long enough and has a large enough viewing angle so that there would be no interference from the solar panels that could block the transmitted signal. The antenna has to be able to point towards Earth during each orbit. Figure 3.2.2 shows all of the different orbit orientations and viewing sectors with respect to Earth during one year.

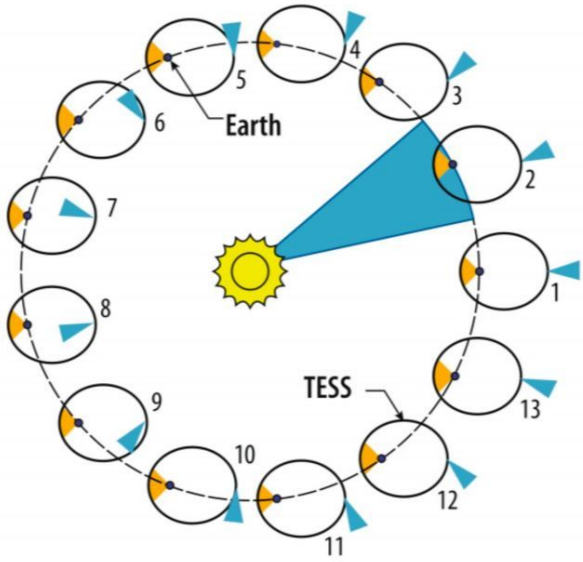

Figure 3.2.2: Orbit orientations and viewing sectors during one year of TESS' orbit: blue triangles indicate the direction of TESS' cameras (always away from the sun) while the orange triangles indicate the parts of the orbit used to downlink information (currently where science operations stop) (*Credit: NASA*)

The final requirement for the antenna positioning mechanism is having a gimbal with two degrees of freedom. It will require two degrees of freedom since we will need the antenna to move side-to-side and up-and-down in order to point towards Earth, but there isn't a need for it to spin.

3.2.3 Trade Study to Identify Ideal Candidate

The aspects we needed to compare and decide on included the model we wanted to base our design on, the material the mast should be made of, the mast design, and the type of gimbal to use.

The two previous satellites that used the mast design we decided on were the JPL NuSTAR and the Shuttle Radar Topography Mission (SRTM) (see Figures 3.2.1a and 3.2.1b). Both the NuSTAR mast and the SRTM mast use the same ADAM-Mast structure, which is a truss structure with 87 cube-shaped sections, or bays. Latches on the diagonal truss members allow the deployment out of the canister [22]. See Figures 3.2.3a and 3.2.3b for a visual.

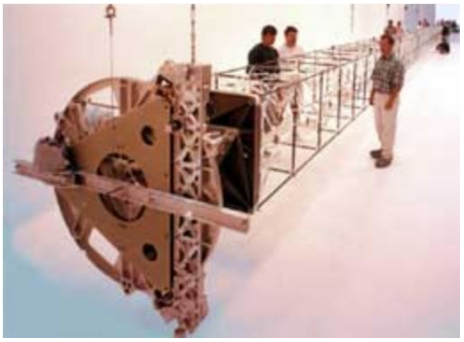

Figure 3.2.3a: SRTM Mast (*Credit: NASA*)

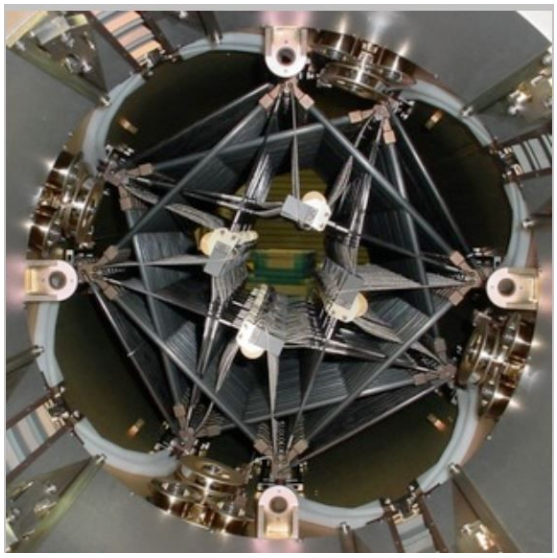

Figure 3.2.3b: NuSTAR Mast (*Credit: NASA*)

We looked at many different types of deployable masts including the CoilABLE mast, shown in Figure 3.2.3a, the collapsible tube mast, and the telescopic mast, shown in Figure 3.2.3b [33]. In the end, we decided to use the ADAM truss mast that spirals out, because that is the type of mast used by the NuSTAR and SRTM. It has been tried and it has proven to work so we have decided that it is the best option for us.

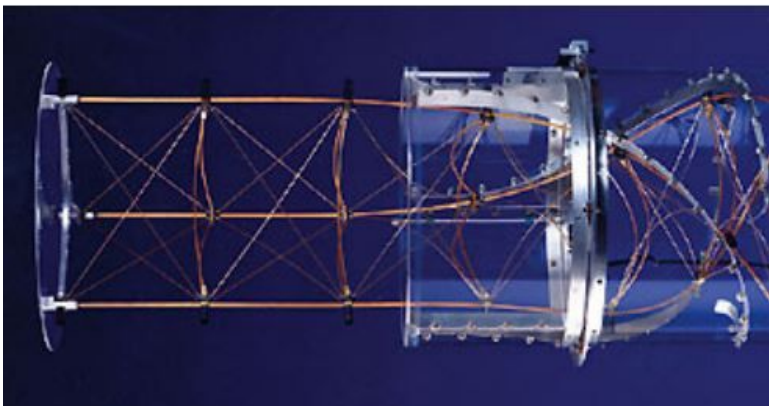

Figure 3.2.3a CoilABLE Mast (credit: [33])

Figure 3.2.3b Telescopic Mast (credit: [33])

The Nustar mast is approximately 10 meters long and the SRTM mast is 60 meters long. Both are made of Invar 36, a 36% Nickel-iron alloy. Since both of these masts worked very well, we have decided to use the same design and material.

Other materials we have considered for the mast include Kevlar and Aluminum. Kevlar is very strong, lightweight, and very resistant to temperature changes. Kevlar has also been used on spacecraft in the past. Aluminum is lightweight and while it is not very strong on its own, aluminum alloys can be used for increased strength [23]. While these both appear to be good options, we have decided to stick with the Invar 36 because that was used specifically for extendable masts before and have proven to work very well.

For our purposes, we have decided to use the MOOG Space and Defense Group Type-22 Antenna Pointing Assembly because it satisfied the size requirements of our design.

3.3 Modification Subsystems: Piezoelectric ACS

The piezoelectric ACS modification is a modification on the ACS subsystem. It will change TESS' attitude control system from four reaction wheels to a piezoelectric sphere.

3.3.1 Reasoning for Piezoelectric Modification Choice

Figure 3.1.1.1: Cylindrical Piezoelectric Actuator size compared to SD card. The red cylinder is the piezoelectric actuator, resting on top of the actuator is the control sphere held in place by a permanent magnet hidden underneath by the actuator. (*Credit: Bakanauskas V. et al.*)

Piezoelectric actuators can make fine adjustments from variable strain due to changing the electric field voltage. The small size of the piezo-actuator, as seen in Figure 3.1.1.1, allowed the possibility of reducing mass at the cost of slower but more accurate attitude control [13]. Based on the research paper by Bansevicius, titled *SYNTHESIS OF TRAJECTORIES IN PIEZOELECTRIC ATTITUDE CONTROL DEVICES FOR NANOSATELLITES*, a small piezoelectric actuator was used with an excitation voltage

of 30 V to oscillate gear-like-teeth in the contacting actuator surface to move a control sphere loosely held by a permanent magnet [11].

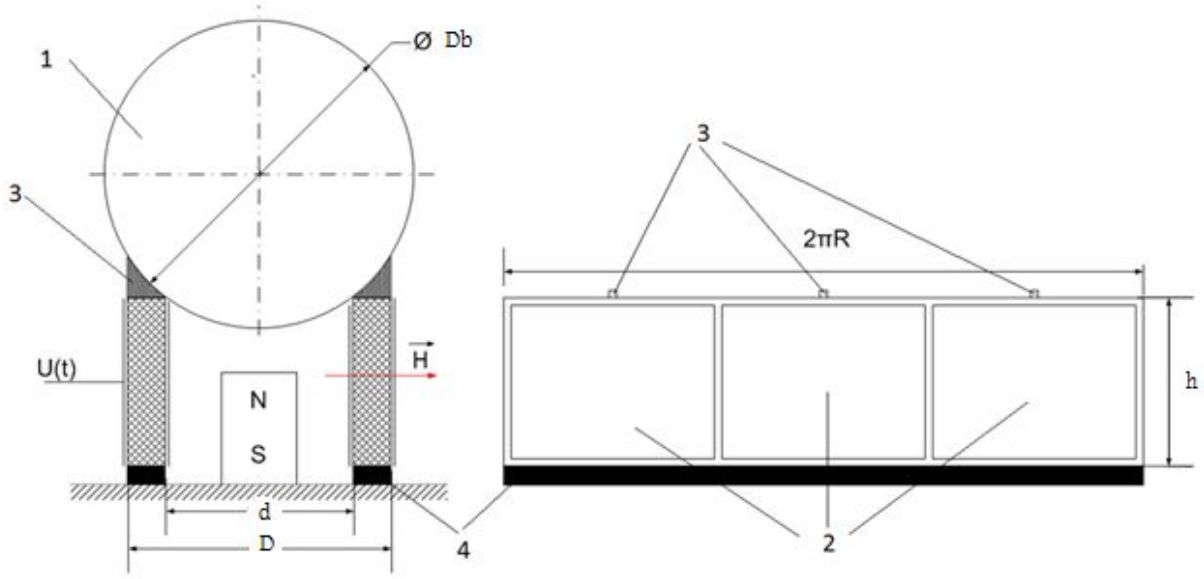

Figure 3.3.1.2: Cylindrical piezoelectric actuator diagram showing the location of the control sphere at 1, the roll out view of the cylinder as a beam at 2, the gear-like-teeth at 3, and the fixed supports at 4. The cylinder is electrically grounded on the inner surface with the electrode on the outer surface. (*Credit: Bansevicius, R. et. al*)

The dimensions of the piezoelectric actuator in Figure 3.3.1.2 tested were for a cylindrical shell with outer diameter of 84 mm, an inner diameter of 70 mm, and a height of 38 mm. The control spheres used were had radii of 71 mm and 86 mm. Based on their results, the optimal force applied by one gear-like-tooth to the smaller 71 mm radius control sphere was 3 kN. The best possible torque of 213 N*m would occur when the force is applied at a right angle to the surface normal vector as seen in Figure 3.3.3.3.

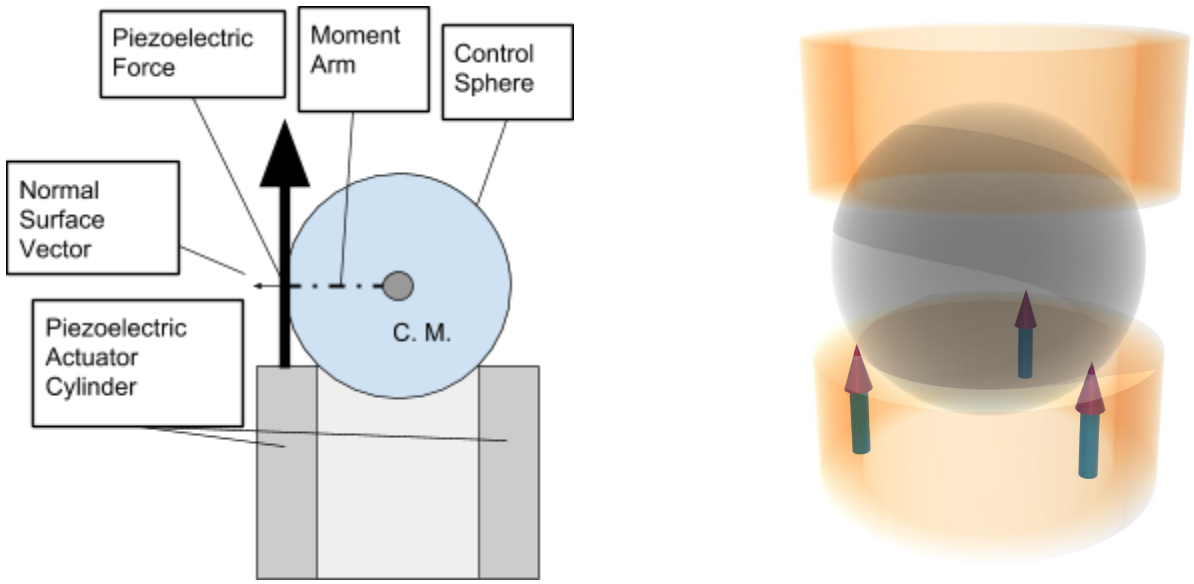

Left Right

Figure 3.3.3.3: Diagram of piezoelectric actuator and applied force to control sphere for optimum torque. The right diagram shows a see-through model showing the application of forces along the equator of the sphere relative to the horizon.

3.3.2 Requirements for Piezoelectric Modification

The requirements for the piezoelectric modification are based on the 4 reaction wheels on TESS. Table 3.3.2.1 on the following page has a summary of the requirements. The Honeywell HR-04 reaction wheel was used to estimate the mass, power, and volume as a comparable reaction wheel to the custom Honeywheel reaction wheels used on TESS [15]. The piezoelectric system will not exceed three-eighths the reaction wheel system mass of 10.4 kg which gives a mass limit of 3.9 kg [14]. The modification will not exceed the reaction wheel system peak system power of 192 W. The total volume of the piezoelectric modification will not exceed 1.78 $x10^{-3}$ m^3 and size will not exceed length, width, and height dimensions of a box 0.320 m x .424 m x 0.258 m. From the experimental results of the research paper by Bansevicius, the best force applied to the control sphere was 3 kN. Applied tangent to the surface normal vector the best torque would be 213 N*m [11].

Table 3.3.2.1: Requirements for Piezoelectric ACS	
Requirement (Units)	**Requirement Quantity**
Max. Mass (kg)	3.9
Max. Volume (m^3)	3.5 x10-2
Max. Voltage (V)	28
Max. Power per Piezo. Unit (W)	77.5
Max. System Power (W)	155
Min. Piezo. Force (N)	352
Min. Torque (N*m)	25

3.3.3 Trade Study to Identify Ideal Candidate

Due to the experimental nature of the piezoelectric attitude control device, off the shelf components for this application do not exist.

To determine the size, power, and force provided by the piezoelectric, piezoelectric materials were compared to determine the ideal material for this application. Materials for the control sphere were compared based on density, in order to optimize size and mass. Ferromagnetic and nonmagnetic materials were considered as well. For the ferromagnetic materials, a comparison of commercial permanent magnets were compared as well. Seen in Table 4.1 of *Vibration Control of Active Structures : An Introduction* the material properties of Lead-Zirconate-Titanate (PZT) and Polyvinylidene fluoride (PVDF) are shown. Due to the proprietary nature of Pz26, the material properties are shown in Table 3.3.3.1 on the following page are under the assumption that it shared the same Young's Modulus and d_{31} value as PZT since Pz26 is a variation of PZT.

Table 4.1 Typical properties of piezoelectric materials

Material properties	PZT	PVDF
Piezoelectric constants		
$d_{33}(10^{-12}C/N$ or $m/V)$	300	−25
$d_{31}(10^{-12}C/N$ or $m/V)$	−150	*uniaxial*: $d_{31} = 15$ $d_{32} = 3$ *bi-axial*: $d_{31} = d_{32} = 3$
$d_{15}(10^{-12}C/N$ or $m/V)$	500	0
$e_{31} = d_{31}/s^E(C/m^2)$	−7.5	0.025
Electromechanical coupling factor		
k_{33}	0.7	
k_{31}	0.3	∼0.1
k_{15}	0.7	
Dielectric constant $\varepsilon^T/\varepsilon_0$ $(\varepsilon_0 = 8.85\ 10^{-12}F/m)$	1800	10
Max. Electric field (V/mm)	2000	$5\ 10^5$
Max. operating (Curie) $T°$ $(°C)$	$80° - 150°$	90°
Density (Kg/m^3)	7600	1800
Young modulus $1/s^E$ (GPa)	50	2.5
Maximum stress (MPa)		
Traction	80	200
Compression	600	200
Maximum strain	Brittle	50%

Table 3.3.3.1: Material Properties of Lead-Zirconate-Titanate (Pz26) Ceramic from Meggit A/S

Ferroperm™ Piezoelectric

Pz26 (Navy I) Hard relaxor type PZT

Material properties

Electrical	Symbol	Pz26
Relative dielectric permittivity at 1 kHz	K_{33}^T	1300
Dielectric dissipation factor at 1 kHz	$\tan\delta$	3×10^{-3}
Curie temperature	$T_C >$	330 °C
Recommended working range	<	230 °C
Electromechanical		
Coupling factors	k_p	0.56
	k_t	0.47
Piezoelectric charge coefficient	d_{33}	300 pC/N
Mechanical		
Mechanical Quality Factor	$Q_{m,t}^E$	>1000
Density	ρ	7.70 g/cm³

Note: Due to continuous process improvement, specifications are subject to change without notice.
Please be aware that extreme dimensions and geometries can lead to exaggeration in tolerances in all materials.

Assumed Young's Modulus (GPa)	50
Assumed d31 (C/N)	-150

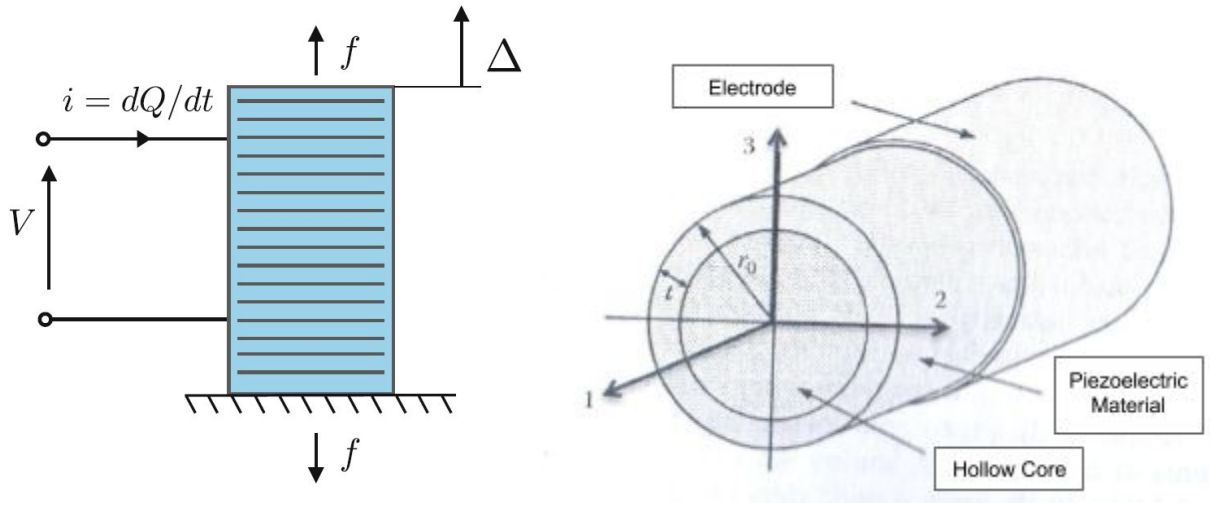

(Left) (Right)

Figure 3.3.3.1: The left figure shows a generic piezoelectric stack actuator where an applied voltage, V, apply a force, f, due to, Δ, the product of the strain, ε, times the number of layers, n, times the their thickness, t. The figure on the right shows a cylindrical piezoelectric shell where the electrode can be applied on the outer face of the piezoelectric shell and the ground electrode can be applied on the inner face of the shell. Both expand the piezoelectric ceramic in the longitudinal direction, up in the left figure and in the 1-direction of the right figure.

$$F = A\varepsilon Y^{\mathrm{p}} = \frac{-E_{\mathrm{tw}} d_{31}}{(r_0/t - 0.5)\ln(1 - t/r_0)} A Y^{\mathrm{p}} = E_{\mathrm{tw}} d^{\mathrm{f}}_{31,\mathrm{eff}} A Y^{\mathrm{p}}$$

Equation 3.3.3.1: Equation for finding the piezoelectric force along the longitudinal axis of the piezoelectric cylinder.

Equation 3.3.3.1 from *Smart Composites: Mechanics and Design* describes the piezoelectric force in terms of the cross sectional area, A, of the piezoelectric shell, the piezoelectric coupling factor, d_{31}, the outer radius of the piezoelectric shell, r_o, the thickness of the piezoelectric shell, t, and the longitudinal Young's modulus, γ^p, for the piezoelectric shell.

$$F = (V/t)(-d_{31})\frac{1}{[(r_o/t - 0.5)\, ln(1 - t/r_o)]} A\gamma^p$$

Equation 3.3.3.2: Expanded piezoelectric force equation accounting for thin wall assumption.

Assuming a thin-wall approximation as seen in Equation 3.3.3.2 shown previously, the electric field, E_{tw}, is defined as the voltage applied on the piezoelectric material thickness, V, divided by the thickness of the material, t. Figure 3.3.3.1 above shows two types of piezoelectric designs considered prior to the trade study, where the left figure shows a stack of many layers of piezoelectric material, while the figure on the right shows a uniform piezoceramic cylindrical shell with a hollow core. The cylindrical piezoelectric actuator was selected as the model for the trade study since it is the type used in the research paper by Bansevicius [11].

Based upon the piezoelectric properties are shown on the next page in Table 4.1 from chapter 4 of Preumont *Vibration Control of Active Structures* in relation to Equation 3.3.3.2, a trade study was conducted where Table 3.3.3.1 on the following page show the results.

Table 3.3.3.1: Piezoelectric Materials for a Piezoelectric Actuator Scaled to 6 cm Radius x 5 cm Height for a 6.5 cm Radius Control Sphere

Property (Units)			
Material:	Pz26	PZT	PVDF
Type:	Ceramic	Ceramic	Polymer
Mass (kg):	0.7	0.69	0.16
Volume (m^3):	5.65 x10-4	5.65 x10-4	5.65 x10-4
Force per Gear-Like-Tooth (N):	4040	4040	20.2
Voltage (V):	28	28	28
Unit Power (W):	72.3	72.3	72.3

Another trade study, shown in Table 3.3.3.2 below, for the control sphere was conducted to find the best material to apply forces from the piezoelectric actuator in order to cause a torque and rotate TESS [28, 34]. To determine the sphere structure from the trade study, the inertia tensors of a sphere and spherical shell were calculated based on the mass of the material and outer radius of the sphere or shell [35].

Table 3.3.3.2: Control Sphere Materials for Control Sphere Scaled to 6.5 cm Radius for 6 cm Radius x 5 cm Height Piezoelectric Actuator			
Property (Unit)			
Material	**Tungsten**	**Beryllium S 65 A**	**Magnesium A 31B**
Density (kg/m3)	19,300	2,000	1700
Solid Mass (kg)	22.2	2.3	1.96
Shell Mass (kg)	4.74	0.49	0.42
I Sphere (kg*m^2)	3.75 x10-2	3.89 x10-3	3.30 x10-3
I Shell (kg*m^2)	1.33 x10-2	1.38 x10-3	1.18 x10-3
Volume (m^3)	6.47 x10-4	6.47 x10-4	6.47 x10-4

4. Analyses

4.1 Major Analysis: Antenna Positioning Mechanism

4.1.1 Goal of Analysis

The goal of the analysis of the antenna positioning mechanism is to find out whether it would be a feasible modification for the purpose of increasing TESS' coverage of the sky. If the gimbal and mast system work properly, without interference, and maintain equilibrium in the overall system, TESS would no longer have to spend 16 hours each orbit solely to make massive attitude adjustments in order to downlink. TESS would now be able to simultaneously perform scientific operations and downlink data (during the original downlink window) and use capture more of the sky and potentially find more exoplanets, without altering the total mission time.

4.1.2 Assumptions, Methods, and Principles

First and foremost, we assume that the spacecraft, with reaction wheels removed, and the added mast and antenna system, will have uniform densities. This allows for an easier centroid calculation for TESS. Next, TESS is assumed to have mass with a rigid

body (with respect to structural integrity) and a flexible appendage.. It is presumed that the mast will extend in the +x direction, as seen in figure 4.1.2.1.

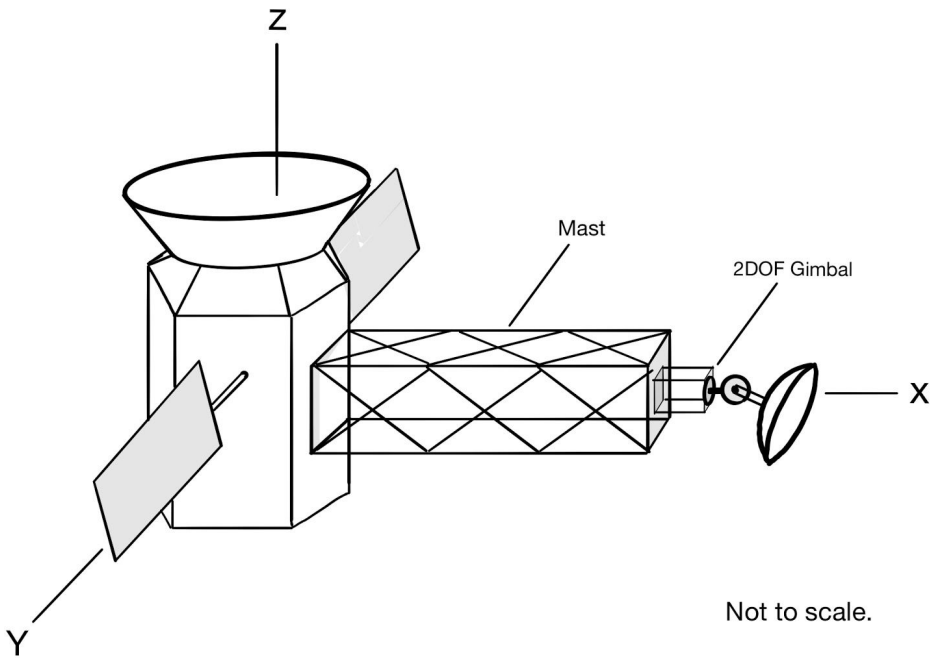

Figure 4.1.2.1: Artist's rendition of TESS showing the modifications as well as the coordinate axis system used for analysis. The X-axis runs through the length of the mast and 2-Degree-of-Freedom gimbal, and the Ka-band parabolic antenna. The Y-axis runs through the solar panel array of TESS. The Z-axis runs through the center of mass of TESS through the observatory section on top.

We assume that there are no magnetic forces enforced, in subsequent calculations and analysis. The observational instruments will always be antisolar (opposite to the sun). It is assumed that the effect of aerodynamic drag is negligible since TESS is in a Highly Elliptical Orbit (HEO).

Once the minimum length and mass of the mast were determined, the gimbal and antenna lengths and masses were estimated based on off-the-shelf components (section 4.3.2).

$$
\begin{aligned}
I_1\dot{\omega_1} &= (I_2 - I_3)\omega_2\omega_3 + T_1 \\
I_2\dot{\omega_2} &= (I_3 - I_1)\omega_1\omega_3 + T_2 \\
I_3\dot{\omega_3} &= (I_1 - I_2)\omega_1\omega_2 + T_3
\end{aligned}
$$

Equation 4.1.2.1: Euler's Equations (Rigid Body Dynamics)

The first step in finding a torque balance was to establish the reference axis as seen previously in Figure 4.1.2.1, where the x-axis would run parallel with the mast, the y-axis run parallel with the solar panels, and the z-axis be orthogonal to both of these axes. The reference origin of these axes is the new center of mass after the mast and gimbal additions.

The length of the mast was a design choice to allow for a turning angle of 240 degrees in the worst-case scenario (to avoid the solar panels). We determined that a length of 1.25m would be optimal.

$$I_{zz} = \tfrac{1}{2}mr^2 \; ; \; I_{xx} = I_{yy} = \tfrac{1}{4}mr^2 + \tfrac{1}{12}ml^2$$

Equation 4.1.2.2 Moment of Inertia for a cylinder, where m is mass, r is radius, and l is length.

$$I_{xx} = \tfrac{1}{12}m(h^2 + w^2) \; ; \; I_{yy} = \tfrac{1}{12}m(l^2 + h^2) \; ; \; I_{zz} = \tfrac{1}{12}m(l^2 + w^2)$$

Equation 4.1.2.3 Moment of Inertia for a rectangular prism, where m is mass, l is length, w is width, and h is height.

$$I_{xx} = \tfrac{2}{3}mr^2 \; ; \; I_{yy} = I_{zz} = \tfrac{5}{12}mr^2$$

Equation 4.1.2.4 Moment of Inertia for a hemispherical shell, where m is mass and r is radius.

In order to simplify the mathematics, it was assumed that the components being added to TESS were generalized shapes. This was due to the inertial moments of generalized shapes being given by Equations 4.1.2.2, 4.1.2.3 and 4.1.2.4 [35]. The original spacecraft would be a cylinder rather than a hexagonal prism, the mast would be a hollow rectangular prism, the gimbol a circular cylinder, and the antenna to be a hollow hemisphere.

$$\frac{\sum m_i \bar{x}_i}{\sum m_i}$$

Equation 4.1.2.6 Center of mass equation, where m_i is the individual mass of each component, and $\bar{x}_i$ is the center of mass of each component.

The new center of mass was found using a basic center of mass formula, equation 4.1.2.6 along with the assumption that all the shapes had uniform density.

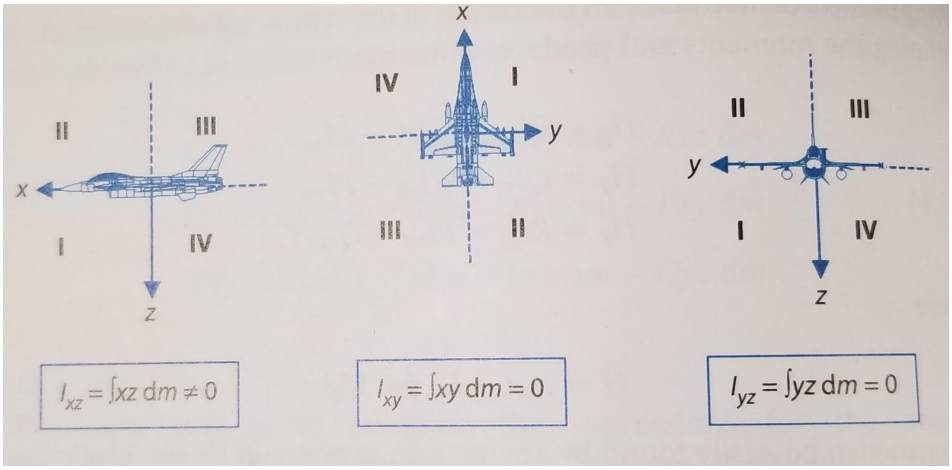

Figure 4.1.2.1: Product inertia explanatory diagrams (Credit: *Introduction to Aircraft Flight Mechanics Performance, Static Stability, Dynamic Stability, Classical Feedback Control, and State-Space Foundations* by Thomas R. Yechout) greatly helped with the understanding of when a product inertia is present and when it was not.

Due to the asymmetry of the spacecraft, a product inertia was developed around the xz-plane. Figure 4.1.2.1 provides insight into the circumstances where a product of inertia develops. This was calculated and compounded to the inertia value with help from the parallel axis theorem. Following finding the inertia, the Euler equation of motion was put together.

$$I_O = I_i + m_i d_i^2$$

Equation 4.1.2.7 The parallel axis theorem. This theorem places the moment of inertia about individual components' centers of mass about the center of mass of the reference point.

After individually calculating the moment of inertia for each subcomponent, the parallel axis theorem, Equation 4.1.2.7, was used to find the subcomponents inertia with respect to the center of mass [35]. From there, the values were all summed together to find the total inertia of the craft.

$$F_{Gravity\ Gradient_i} = m_i \frac{(v^2(r+\bar{x}cos(\theta))-\mu)}{(r+\bar{x}cos(\theta))^2}$$

Equation 4.1.2.8 The Gravity gradient force equation. m_i is the mass of the body, r and v correspond to the radial distance from Earth and its orbital velocity, respectively. $\bar{x}$ denotes the body's center of mass' distance from the center of mass of the total system. θ is it's vertical angle, and μ is the standard gravitational parameter of Earth.

The next component of work for the design process was finding the influence of solar pressure and gravity gradient added to the craft due to the mast. The torques on the spacecraft due to these forces were considered. Using Equation 4.1.2.8, we found the gravity gradient force on TESS' solar panels and bus portion of the craft, and then found the gravity gradient force exerted on the gimbal and antenna portion of the spacecraft. If the force is multiplied by its distance from the center of mass, the torque is calculated. Finally, since the solar radiation pressure at 1AU is around 9.08 $\mu N/m^2$, the torque due to it would be extremely small in magnitude (~10^{-6} Nm), and its effect on the spacecraft would be negligible. However, it was considered in the simulation.

Finally, a statics approach was used to sum the moments together and evaluate an equilibrium moment balance. By dividing the craft into three planes, xy,xz, and yz, we came up with the moment equilibrium equation for each axis.

4.1.3 Math, Models, and Code

After the method was followed through, the values for the moment of inertia in each axis as well as the product inertias were found for the total spacecraft about its center of mass using Equations 4.1.2.3, 4.1.2.4, 4.1.2.5, and 4.1.2.7.

Table 4.1.3.1: Inertia Tensor Values for the Modified TESS			
Inertia (kg m^2)	Value	Inertia (kg m^2)	Value
Ixx	140.8508434	Ixy	0
Iyy	105.7106372	Iyz	0
Izz	12.28384975	Ixz	0.05852442093

From the data on Table 4.1.3.1, one can draw the conclusion that the craft is more resistant to turning about the x and y axis. While the craft has a slight product of inertia, it does not greatly hinder the crafts spin in the xz-plane.

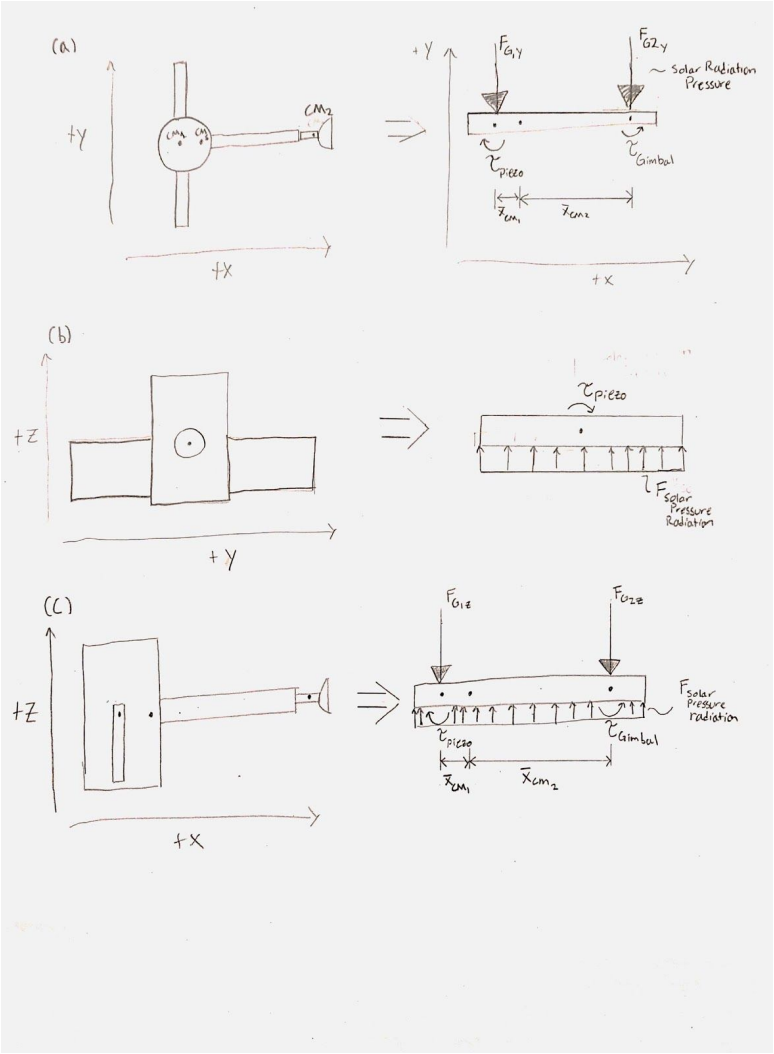

Figure 4.1.3.1 This figure shows how each plane can set up its own equilibrium problem.

Splitting the spacecraft into three equilibrium problems became the best way to find the effects of different torques on TESS. As shown in Figure 4.1.3.1, it becomes easy to see how the gravity gradient, gimbal torque, and the solar wind pressure affect the craft in each direction. Once each individual axis had been balanced, we compiled the torques we would need in each axis in order to maintain equilibrium over the orbit.

$$\sum M_z = 0; \quad \tau_{piezoelectricX} + \tau_{GimbalX} + (F_{Gravity\ Gradient\ Mass1Z}\bar{x}_{Mass1Z} - F_{Gravity\ Gradient\ Mass2Z}\bar{x}_{Mass2Z}) = 0$$

Equation 4.1.3.1 Sum of the moments about the z-axis, assuming equilibrium. Equation deduced from Figure 4.1.3.2a. For clarification, τ_{Gimbal} is the torque the gimbal provides, and $\tau_{piezoelectric}$ is the torque needed to be provided by the piezoelectric attitude control system.

$$\sum M_x = 0; \quad \tau_{piezoelectricX} + \tau_{Solar\ Radiation\ Pressure} = 0$$

Equation 4.1.3.2 Sum of the moments about the x-axis, assuming equilibrium. Equation deduced from Figure 4.1.3.2b.

$$\sum M_y = 0; \quad \tau_{piezoelectricY} + \tau_{GimbalY} + (F_{GGM1Y}\bar{x}_{M1} - F_{GGM2Y}\bar{x}_{M2}) + \tau_{SRP} = 0$$

Equation 4.1.3.3 Sum of the moments about the y-axis, assuming equilibrium. Equation deduced from Figure 4.1.3.2c.

After formulating the equilibrium equations, equations 4.1.3.1, 4.1.3.2, and 4.1.3.3, they were plugged into MATLAB for a simulation of how the craft would move over the orbit [37]. This simulation gave us the magnitude of torque that the piezoelectric ACS would need to provide in each axis in order to have zero attitude change, for the worst-case scenario.

Functions were created to describe the torques on the spacecraft about the 3 axes. These functions describe the torque on the spacecraft (either a disturbance torque or a controllable torque by an onboard component), and hence give us the resultant

counter-torque needed to be effected by the piezoelectric. All torques are described as functions of the true anomaly of the orbit.

4.1.4 Results

Here is an illustration to depict the coordinate axes that we based our calculations, simulations and results upon.

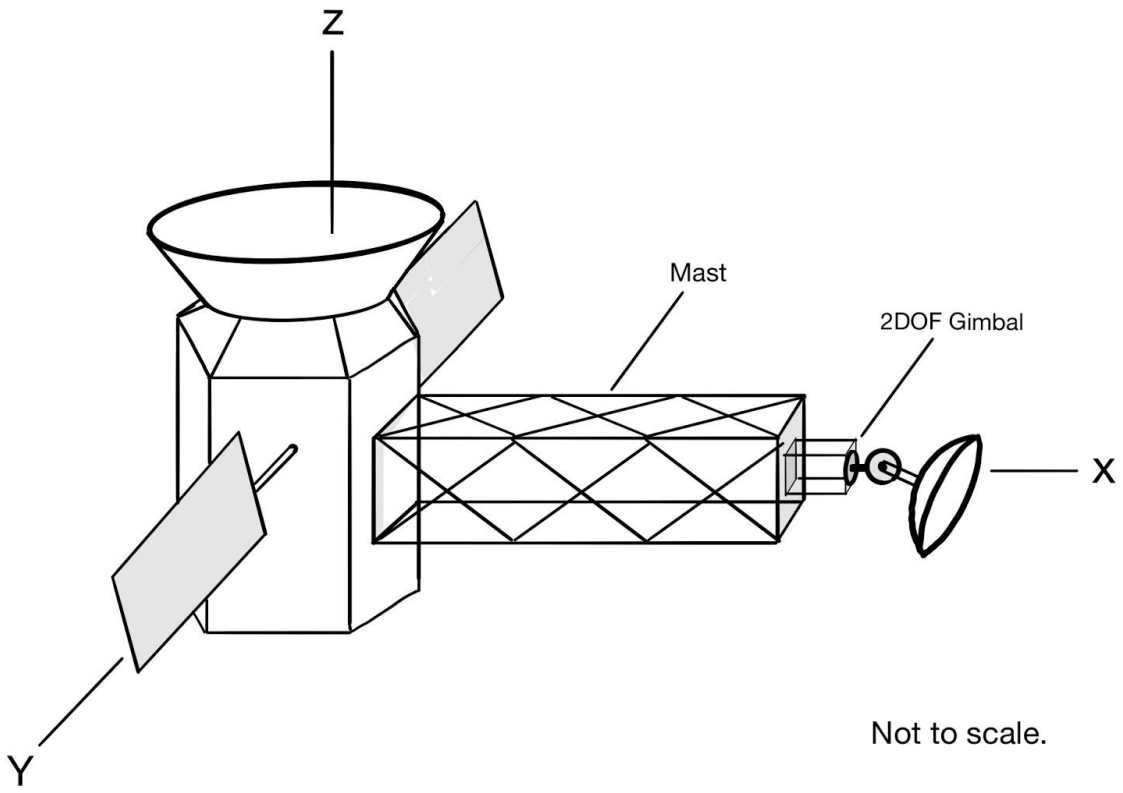

Figure 4.1.4.1: Coordinate Axes of Illustration

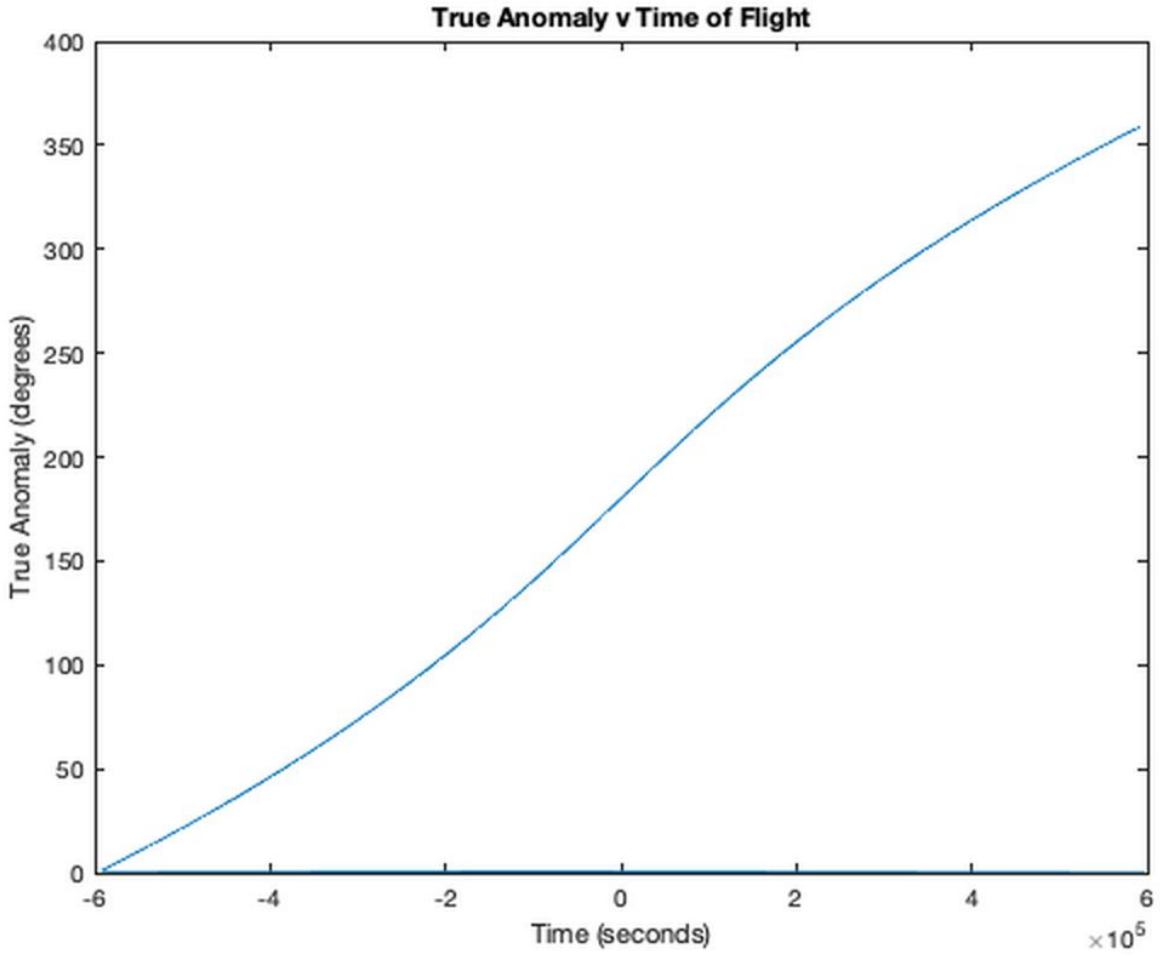

Figure 4.1.4.2: True Anomaly vs Time of Flight

Figure 4.1.4.2 describes the relationship between the time-of-flight of the spacecraft in the orbit and its true anomaly. The simulation was run for one full orbit. Time '0' represents the time at which the spacecraft is at the apogee (since a 0 degree true anomaly represents the true anomaly at the perigee). The noticeable warping or non-linearity is due to the fact that the orbit is elliptical.

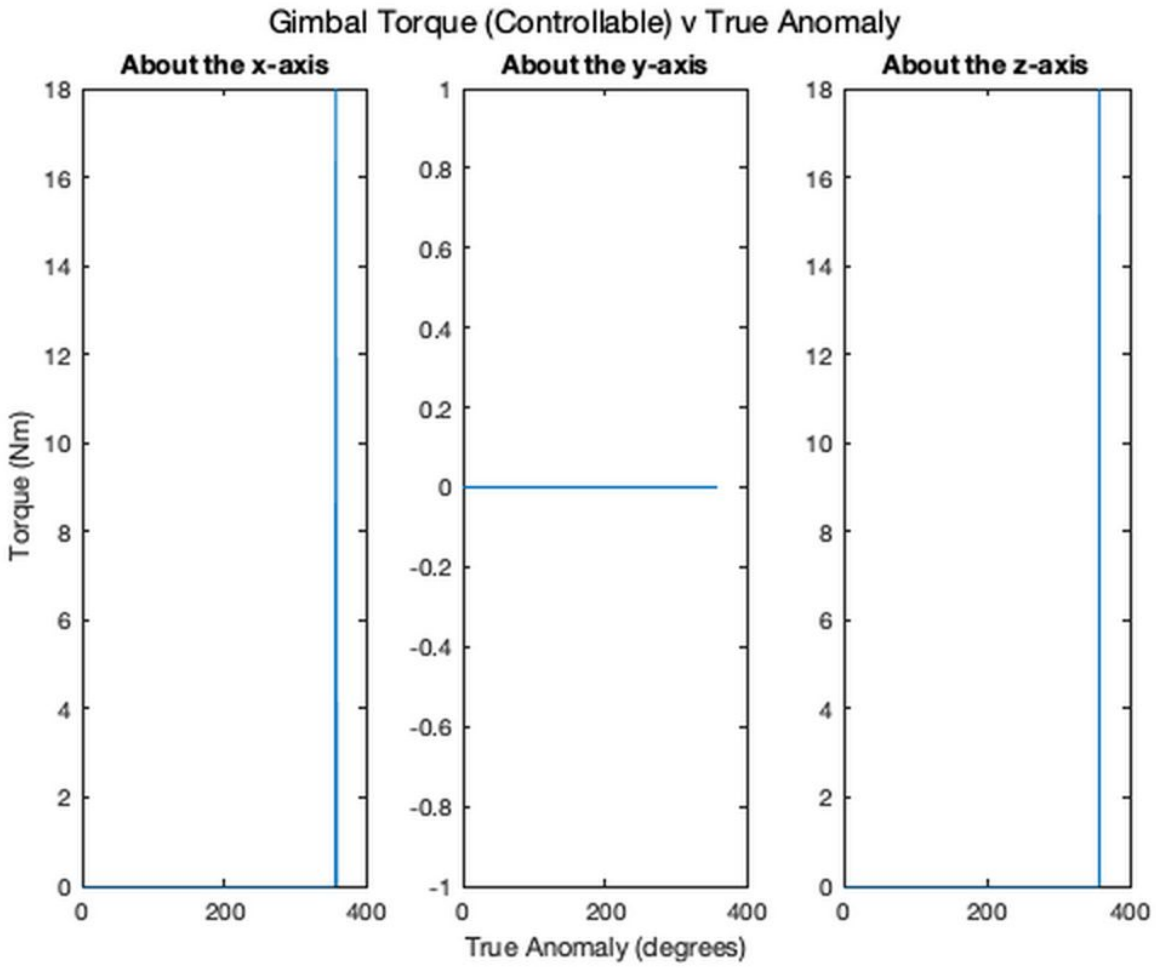

Figure 4.1.4.3-Gimbal Torque vs True Anomaly

Figure 4.1.4.3 describes the gimbal torques about the x, y and z axes. These are controllable torques, and we consider the worst-case for our simulation, in order to get the upper bound on the torque needed to be effected by the piezoelectric system in order to maintain equilibrium. Since we have chosen a two degrees of freedom gimbal, we consider the torques about the x and z axes.

The minimum output torque of the MOOG Type-22 Antenna Pointing Assembly is 18 Nm. Hence, we consider an impulsive torque of 18 Nm each about the x and z axes at a true anomaly of 359 degrees, which is when TESS would approach the downlink window. This would also describe the worst-case scenario, in terms of the controllable torques that can be applied.

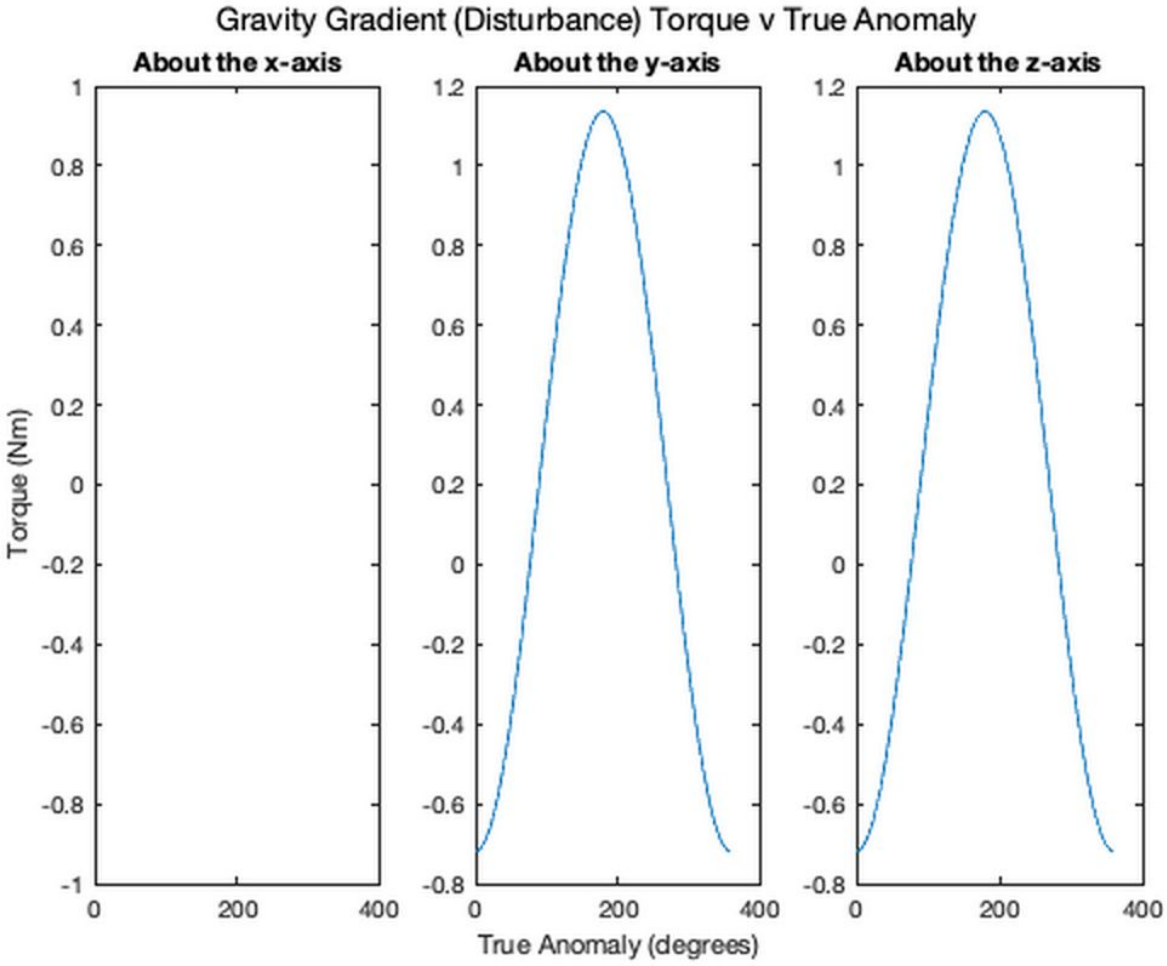

Figure 4.1.4.4: Gravity Gradient Torque vs True Anomaly

Figure 4.1.4.4 describes the disturbance torques on the spacecraft due to the gravity gradient, as a function of the true anomaly. For a fixed orientation of the spacecraft (mast along the velocity vector), the gravity gradient torque would be pronounced about the y and z axes.

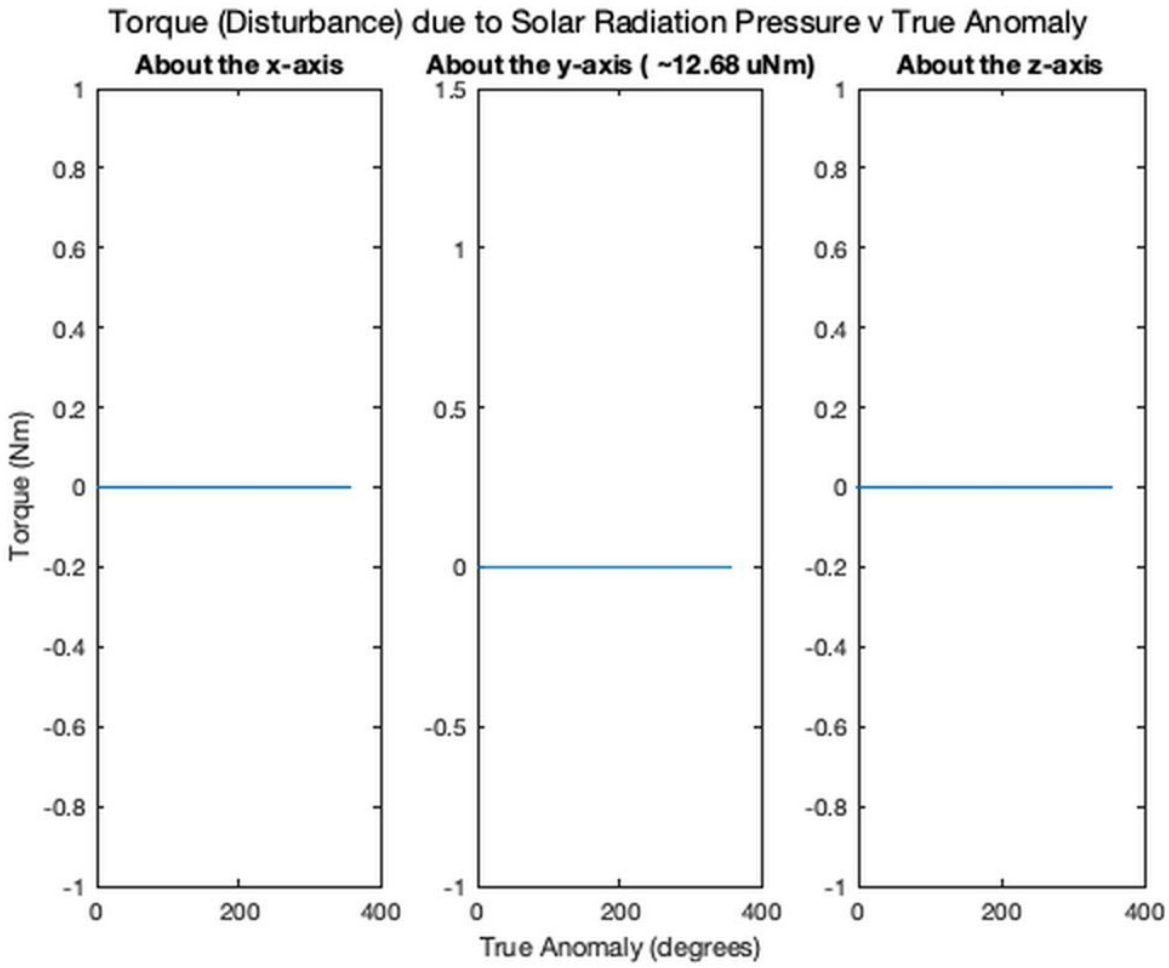

Figure 4.1.4.5: SRP Torque vs True Anomaly

With the assumption that the onboard cameras on TESS always point in a direction opposite to the sun and that the solar radiation pressure is a constant throughout the orbit, the solar radiation pressure would be more pronounced on the 'bottom' surface of TESS, thus imparting a torque about the y-axis. This torque is of a very small magnitude (~12.68 μ Nm) and its effect on the spacecraft is negligible. This can be seen in Figure 4.1.4.5. However, we chose to include it in our simulations to be as accurate as possible, given the assumptions.

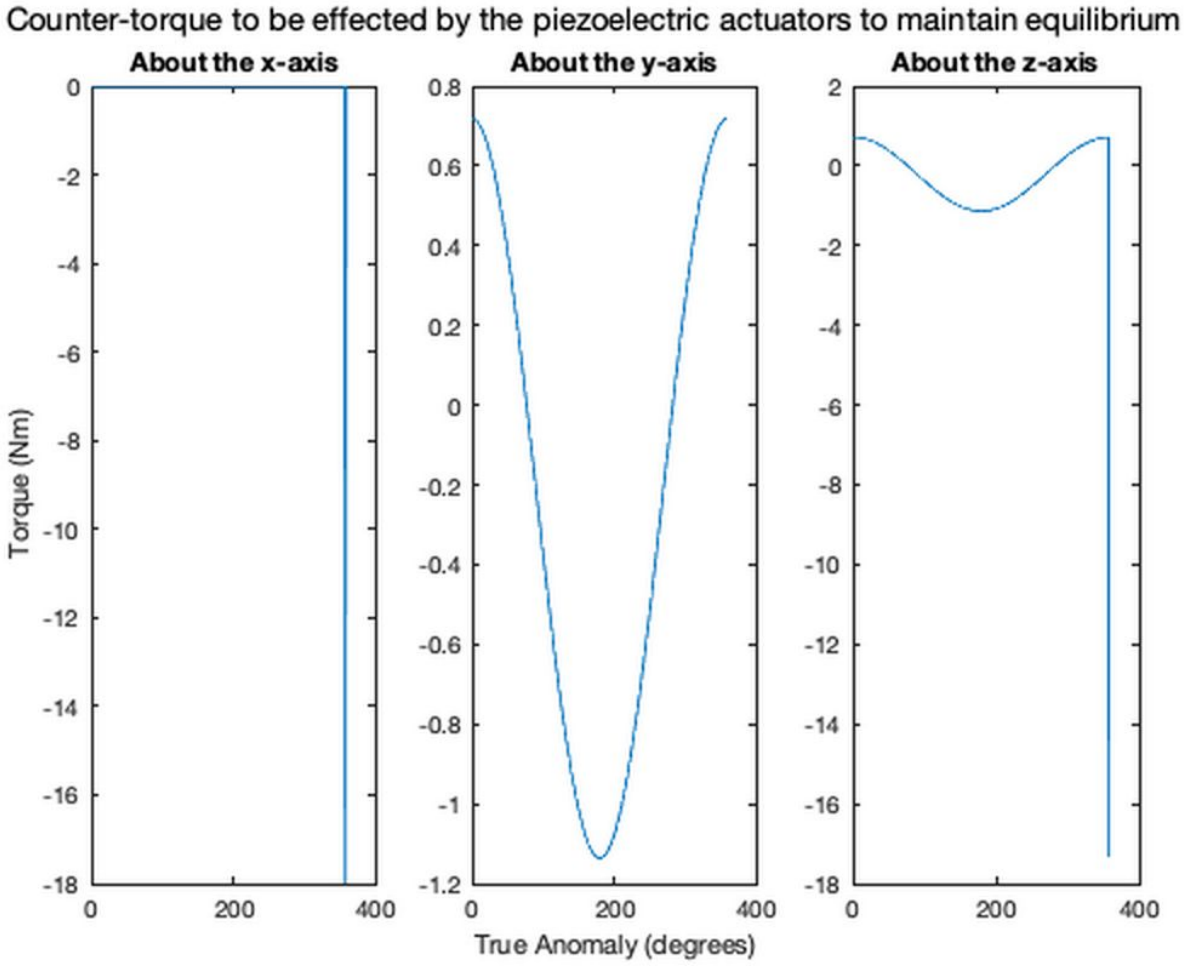

Figure 4.1.4.6: Counter-torque to be affected by the piezoelectric actuators to maintain equilibrium

Figure 4.1.4.6 describes the counter-torques to be effected by the piezoelectric system in order to maintain equilibrium. These are equal to the combined effect of the previous torques in magnitude, and opposite to them in direction.

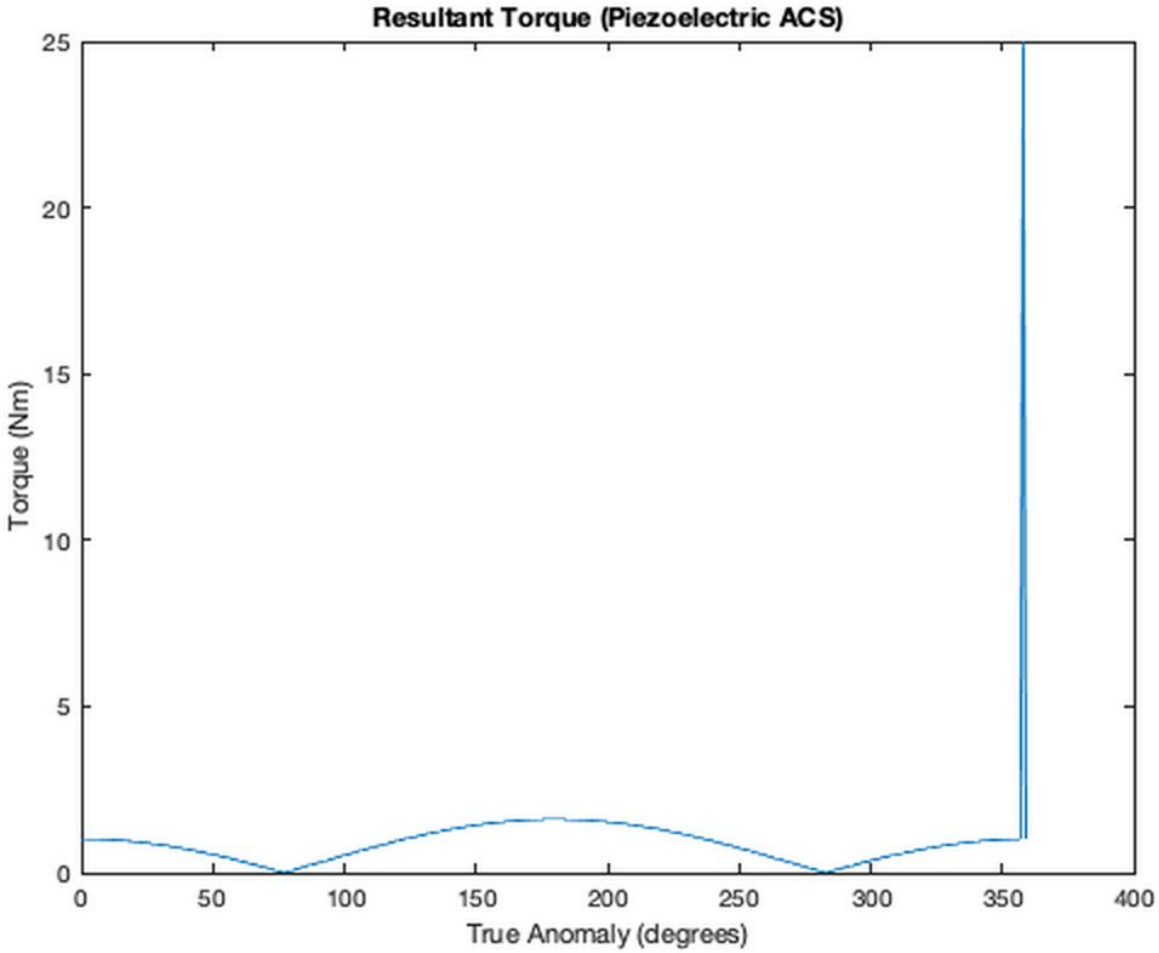

Figure 4.1.4.7: Resultant Torque

Figure 4.1.4.7 describes the resultant counter-torque to be applied by the piezoelectric system in order to maintain equilibrium. For this case (“worst-case”, due to impulsive gimbal torques), the maximum torque needed to applied by the piezoelectric attitude control system is 24.9635 Nm. If the piezoelectric system can impart a torque equal to or greater than this value, it would meet the mission requirements.

4.1.5 Importance

Based on the above results, the antenna mast makes for a suitable modification to meet the mission requirements. Despite the vast oversimplifications involved, the team concluded that it would work within the system. Therefore, it can eliminate the requirement of reorientation towards Earth in order to downlink, by allowing for simultaneous scientific operations and downlinking, which would allow for more of the sky to be observed, without increasing the mission time.

4.2 Minor Analysis: Piezoelectric ACS

4.2.1 Goal of Analysis

The goal for analysis of the piezoelectric attitude control system is to find the mass, power, volume, size, force, and torque to determine if the system is a viable alternative to the original 4 reaction wheels on TESS.

4.2.2 Assumptions, Methods, and Principles

The piezoelectric motor will be analyzed as a linear homogeneous actuator to get a general idea of the forces produced during use. In actuality, the oscillation is nonlinear since the oscillation occurs in a circular cross section thus, the Euler-Bernoulli beam theory should be considered in future analysis. The cylinder will be modeled as a tube since the middle will support the sphere. The sphere will be modeled as a homogeneous spherical shell. The center of mass for TESS will be assumed at the geometric center of the hexagonal prism. All inertia tensor terms will be based on the center of mass of TESS. For calculation of the piezoelectric force, of equation 3.3.3.2, it was assumed that the fraction containing a natural logarithm converted GPa to Pa. Without this assumption, the equation for piezoelectric force from plugging in base units would produce force values that are unreasonably high compared to the experimental results in the research paper of Bansevicius [11].

4.2.3 Math, Models, and Code

The total piezoelectric force was analysed using Equation 3.3.3.2. To find the force of each of the 3 gear-like-teeth, and trim the theoretical value closer to the experimental the following equations 4.2.3.1 and 4.2.3.2 were used.

$$\gamma^{multi} = \gamma^{p} v$$

Equation 4.2.3.1: Young's Modulus adjustment by volume ratio to account for hollow core, where γ^{p} is the piezoelectric Young's Modulus and v is the volume ratio of the piezoelectric to the total volume of a solid cylinder.

$$F/3 = F = (V/t)(-d_{31})\frac{1}{[(r_o/t-0.5)\, ln(1-t/r_o)]} A\gamma^{p} \; (1/3)$$

Equation 4.2.3.2: Piezoelectric force for 1 of 3 gear-like-teeth accounting for hollow core.

The mass requirement of 3.9 kg was based on the size and density of the piezoelectric material chosen from the trade study in section 3.3.3.

The power requirements were found based on the average mission power consumption of 290 W. Subtracting the 192 W of power used by the 4 reaction wheels and adding the 37 W of power used by the mast gimbal system to get 135 W used by other systems. Thus, by subtracting 135 W from 290 W we get 155 W of power available to the piezoelectric system without exceeding the average mission power rate.

$$Izz = (2/5) * m * r^2$$

Equation 4.2.3.3: Inertia formula for a sphere, where m is mass and r is the radius of the sphere.

$$Izz = (2/3) * m * r^2$$

Equation 4.2.3.4: Inertia formula for a spherical shell, where m is the mass and r is the outer radius of the shell

The inertia tensor for the control sphere was found using Equation 4.2.3.3 and 4.2.3.4 above, for a sphere and spherical shell to determine which design to implement.

4.2.4 Results

The Piezoelectric ACS was chosen to be made using PZT for the piezoelectric material and Beryllium S65 A for the control sphere material. The mass, as seen in Table 4.2.4.1 below, of the designed system is 3.68 kg which is smaller than the max mass of 3.9 kg. The max power draw to change the attitude of TESS is 144.7 W, which is due to 28 Volts times 2.58 Amps. The size of the system occupies a volume of 1.78 $x10^{-3}$ m^3. and a box size of 0.32 m x 0.424 m x 0.258 m. The force produced during attitude control is 4040 N which corresponds to a torque of 262 N*m. The solid sphere has an inertia tensor of 3.89 $x10^{-3}$ kg m^2.

Table 4.2.4.1: Piezoelectric ACS Results		
Property (Units)	**Candidate and Properties**	**Requirement**
Piezoelectric Material	*PZT*	N/A
Control Sphere Material	*Beryllium S 65 A*	N/A
Control Sphere Type	*Solid Sphere*	N/A
Total Mass (kg)	*3.68*	< 3.9
Volume (m^3)	*1.78 x10-3*	< 3.5 x10-2
Voltage (V)	*28*	≤ 28
System Power (W)	*144.7*	< 155.0
Piezo. Force (N)	*4040*	> 352
Torque (N*m)	*262*	> 25

4.2.5 Importance

Based on the above results, the piezoelectric ACS meets the design requirements, however the feasibility of the modification to meet the mission requirements is lacking due to the piezoelectric force equation assumption that the natural log term in the denominator acts as a conversion factor from GPa to Pa. Furthermore, there is a 54% difference in the piezoelectric force result and the experimental force result.

4.3 Minor Analysis: Power, Mass, and Volume Change

4.3.1 Goal of Analysis

The goal of the power, mass, and volume change analysis is to find out what impact our modifications would have on the initial system. We need to find out if exchanging

TESS's four reaction wheels with the piezoelectric system saves enough mass to make up for the added mass of the antenna positioning mechanism. We also need to find out what the new overall volume of TESS would be when fully extended and how the collapsable mast would fit inside of TESS when collapsed. FInally, we need to see if the overall system would be consuming more or less power from TESS and what this would mean for the total cost of the project.

4.3.2 Assumptions, Methods, and Principles

From the data of our chosen gimbal, the MOOG Space and Defense Group Type-22 Antenna Pointing Assembly, we know that this gimbal draws 15 W per axis and we have two axes so the antenna positioning mechanism will draw an additional 30 W of power. For the power drawn by deployment of the mast, we found the power drawn for a similar mast, the Canister AstroMast, and used 7 W as an approximation [32].

The amount of power we were aiming to achieve with the piezoelectric system was based on the amount of power the reaction wheels were already drawing.

The mass of the gimbal is 5 kg, found on the datasheet of the MOOG Type-22 gimbal. The mass of the mast was approximated as 7.5 kg, which was calculated by using the ratio of the length to the mass of the SRTM mast and the calculated length of our mast.

In order to use the inertial tensor equations, we had to find out the required length of the extended antenna mast and the mass of the overall system. We found the required length of the mast by first taking into account the viewing angle necessary of the gimbal in order to avoid interference with TESS' solar panels. We found that the mast needs to be at least 1.25 m. The chosen size for the height and width of the mast are both 0.25 m.

4.3.3 Math, Models, and Code

The antenna positioning mechanism increased power consumption by the amount the gimbal draws added to the amount required for deployment of the mast.

In order to find the power change with the implementation of the piezoelectric actuators, we subtracted the power required from the four reaction wheels and added the power required by the two piezoelectric actuators.

The mass added by the antenna positioning mechanism was found by simply adding up the mass of the mast and gimbal.

The mass saved by the piezoelectric actuators was calculated by subtracting the total mass of the four reaction wheels and adding in the mass of the two piezoelectric actuators.

The added external volume of the antenna positioning mechanism was calculated by adding the volumes of the mast and gimbal. The volume of the mast was calculated by multiplying the decided values of 0.25 m for the height and width by the calculated length of the mast.

The added volume of the piezoelectric actuators is not related to this analysis because we are only interested in the external volume of TESS. The piezoelectric actuators replacing the reaction wheels are all inside of TESS and, therefore, do not change the total external volume. The only thing we had to check was that the piezoelectric actuators' volume was at least less than that of the reaction wheels to ensure it can fit inside of TESS and piezoelectric systems are very small so they fit easily.

Tables 4.3.3a through 4.3.3.c show the calculated differences in power, mass, and volume, respectively.

Table 4.3.3a-Total Power Added and Subtracted by Each Modification as well as the Total Power Change

	+ Power	**- Power**	**Total**
Antenna Mod	37 W	----------	+37 W
Piezoelectric	144.7 W	192 W	-47.3 W
Total Change	----------	----------	-10.3 W

Table 4.3.3b-Total Mass Added and Subtracted by Each Modification as well as the Total Mass Change (Masses Taken Before Launch)			
	+ Mass	**- Mass**	**Total**
Antenna Mod	12.5 kg	----------	+12.5 kg
Piezoelectric	+3.7 kg	-10.4 kg	-6.7 kg
Total Change	----------	----------	+5.8 kg

Table 4.3.3c-Total External Volume Added and Subtracted by Each Modification as well as the Total External Volume Change			
	+ Volume	**- Volume**	**Total**
Antenna Mod	7.8125×10^{-2} m^3	----------	7.8125×10^{-2} m^3
Piezoelectric	0 m^3	0 m^3	+0 m^3
Total Change	----------	----------	$+7.8125 \times 10^{-2}$ m^3

4.3.4 Results

Overall, the total power was decreased by 10.3 W, the total mass was increased by 5.8 kg, and the total external volume was increased by 7.8125×10^{-2} m^3. The increased volume may result in complications during launch such as difficulty in getting TESS on the launch vehicle. The increased mass would increase the total cost of getting TESS to orbit, but the reduced power requirement could save some money. Even if the overall change was an increase in cost, it might be worth it, considering the new capabilities we are giving TESS.

4.3.5 Importance

The results demonstrated that it was possible to meet the designs mass, power, and volume requirements with limited information and simplifying assumptions.

5. Test Plans for Analyses

5.1 Tests for Antenna Positioning Mechanism

5.1.1 Necessary Data

Our main concern for the antenna positioning mechanism modification is the structural integrity of the system since it changes the overall structure of the satellite. Vibration and acoustic testing is necessary, especially tests emulating launch conditions, because the satellite will be subjected to massive amounts of vibrations and the individual components of the mast may break or come apart. In addition, we need to ensure the ADCS system is able to correct for the inertia change in the overall attitude control.

5.1.2 Necessary Instruments and Facilities

In order to perform the above tests, we will need to perform a Random Vibration Test, a Sine Sweep Vibration Test, an Acoustic Test, and structural functionality testing (deployment tested with a test model).

In order to perform these tests, we will need a test model of the mast so that we don't have to perform many tests on the real one that that is to be sent into space. For the Random Vibration Test and the Sine Sweep Vibration Test, we will go to Kennedy Space Center's Vibration Lab as they have experience in performing a wide variety of vibration tests for many launch environments, including the SpaceX Falcon 9. Figure 5.1.2a shows the typical closed loop vibration test system used in the KSC Vibration Lab [19].

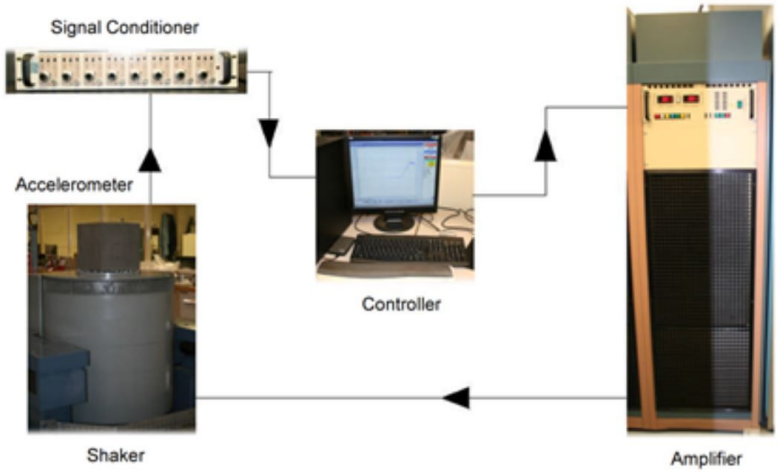

Figure 5.1.2a: Typical Closed Loop Vibration Test System used at Kennedy Space Center Vibration Lab (*Credit: NASA*)

For testing structural functionality as well as well as integration testing, we will go to the Kennedy Space Center Prototype Development Laboratory. Their team works on the design and fabrication as well as testing. This lab will be very useful in testing the mast before we integrate it into the rest of the satellite. The KSC PDL has a machine shop with CNC machines, 3D digital scanning, LabVIEW software programming, and data acquisition that we will use in order to design, simulate, build, and test the antenna positioning mechanism. The LabVIEW software program will be helpful in testing the feedback controller [20].

For the acoustic testing, we will take the mast to the Goddard Space Flight Center Acoustic Test Facility, which consists of a reverberant chamber, acoustic horns, noise generators, a control console, and a data acquisition system. This test facility can test satellites, subsystems, and components [21]. Figure 5.1.2b shows some of these tools.

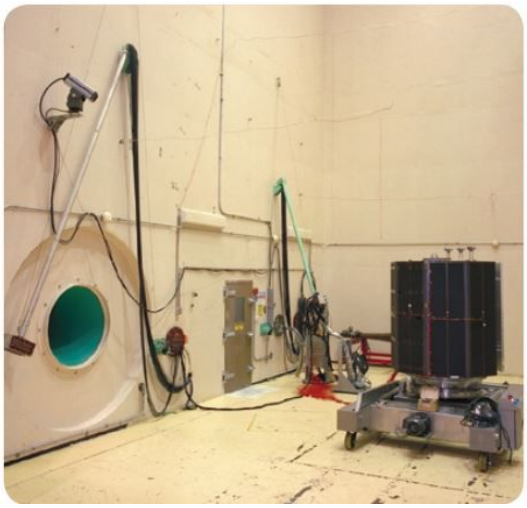

Figure 5.1.2b: Tools used at the Goddard Space Flight Center Acoustic Test Facility (*Credit: NASA*)

5.1.3 Possible Shortcomings and Potential Impact

Failure of the vibrational and acoustic testing could result in the complete failure in functionality of the mast. If one link of the antenna positioning mechanism breaks under vibration, the gimbal and antenna system may separate from the satellite or become stuck in one position. If the feedback controller doesn't work, the total attitude of the spacecraft will be affected. Without being able to accurately and precisely control the overall attitude of the satellite, we may not get the correct data.

5.1.4 Significance of Failure

If the testing shows that the mast will fail or break apart, then this will be fatal to the mission since a broken mast results in a potentially broken, detached, or stuck gimbal and antenna system, which results in loss of capability to downlink data to the Earth. Without the data, the entire mission of TESS fails.

5.2 Tests for Piezoelectric ACS

5.2.1 Necessary Data

Since the Piezoelectric attitude control system has not been tested outside of the earth's atmosphere. Several tests are required to determine the capabilities of the system for attitude control. It is vital for the precision, accuracy, and slew rate of the system to be more than capable of TESS' requirements.

Circuit analysis is needed so that data regarding the piezoelectric devices response to an AC Voltage is needed to accurately control the system. The piezoelectric system can be modeled as a resistor and two capacitors which change in capacitance based on the vibrational frequency.

5.2.2 Necessary Instruments and Facilities

The test bed for measuring the attitude adjustment characteristics of the Piezoelectric ACS is comprised of a spherical air bearing and a weighted system for negating the effects of gravity, as well as a helmholtz coil array for simulating the earth's magnetic field. The piezoelectric device will undergo acoustic testing in order to ensure it will survive the launch into space.

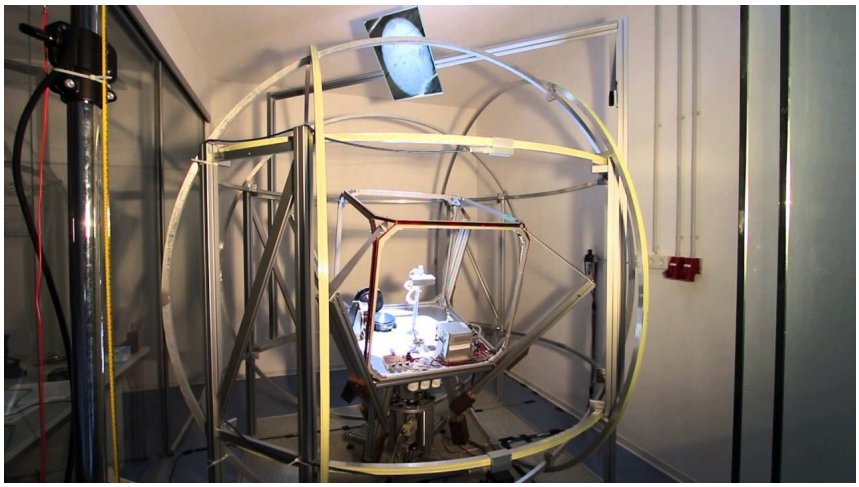

Figure 5.2.2a: Gimbal used at the German Aerospace Center Facility for Aerospace Control Center

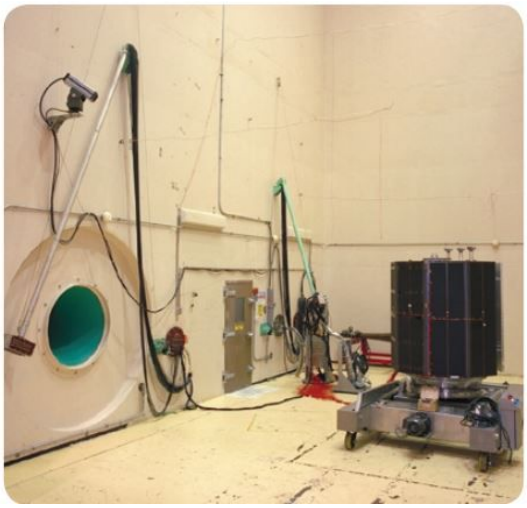

Figure 5.2.2b: Tools used at the Goddard Space Flight Center Acoustic Test Facility (*Credit: NASA*)

5.2.3 Possible Shortcomings and Potential Impact

If the piezoelectric ACS System can not effectively adjust the satellite, TESS will not be able to accurately collect data using the CCD array. If the CCD array can not collect any usable data, than the mission can not be completed.

5.2.4 Significance of Failure

The failure of the Piezoelectric ACS could result in failure of the mission since not being able to accurately control attitude would mean the data being collected would not be accurate and TESS may not even be able to downlink data if the orientation is off. Without the capability to properly orient the satellite, the cameras and solar panels will be off, resulting in errors in data retrieval.

5.3 Tests for Power, Mass, and Volume Changes

5.3.1 Necessary Data

We need to know how our modifications will change the power consumption, mass, and volume of the overall system.

5.3.2 Necessary Instruments and Facilities

In order to determine the overall mass change, the simplest way would be to weigh the satellite with all modifications made. We would need a scale for this.

The overall external volume should be the same during launch since the mast is being stored within the satellite and only being deployed once TESS has reached final orbit. The external volume will increase once TESS reaches its final orbit and the mast is deployed, but it will simply increase by the volume of the mast, gimbal, and antenna system, which we know from design. It could be measured at testing facilities. The internal volume will change as well since we are replacing the reaction wheels with the piezoelectric system, but the change of internal volume has no significance to our analyses as it will not affect any of the mission operations.

The power consumption can be measured at a test facility.

We need to test how our calculated results for power, mass, and volume compare to the actual values after the modifications have been made.

5.3.3 Possible Shortcomings and Potential Impact

Having an increased mass and power consumption results in a more expensive satellite and launch, while decreasing these would result in a cheaper satellite and launch. Each extra kilogram sent into space costs $20,200, so a mistake in mass calculation could cost the stakeholders a large amount of money potentially.

Having a larger volume at launch may result in difficulties in attaching the satellite to the launcher or increase cost as a larger ferring would potentially by needed.

5.3.4 Significance of Failure

While there aren't exactly tests or ways in which this analysis could "fail," having too much mass or power consumption increase may result in a more expensive launch. The total volume during launch is not being affected since we have decided to store the mast in the satellite and have it deploy once TESS reaches its final orbit. In addition, since the length of the mass was decided intentionally so that there would be no interference with the rest of the satellite, there is no way the mission could "fail" due to power, mass, or volume change.

6. Conclusion and Discussion

6.1 Conclusions about the Antenna Positioning Mechanism

6.1.1 Technical Summary of New and Lost Capability of TESS

WIth the antenna positioning mechanism modification, TESS has gained the capability to increase its sky coverage by 1.65% by simultaneously gathering and downlinking data. This capability was achieved using many assumptions that may not actually be acceptable to make. With our evaluation, there are no lost capabilities of TESS' functions.

With both the antenna positioning mechanism modification and the piezoelectric actuator modification, TESS will be able to successfully observe and downlink near the perigee portion of the orbit.

6.1.2 Strengths and Weaknesses of New Design

The main strength of TESS' new antenna positioning mechanism is that it increases TESS' sky coverage, allowing us to improve on the mission requirements.

Weaknesses of this modification include an increased mass and power consumption and therefore an increased cost. In addition, there is an increased external volume, which could cause complications in TESS' launch. Weaknesses of the analysis of this modification include the many assumptions we made in order to simply analyze the mast modification.

6.1.3 Verdict on Antenna Positioning Mechanism

Overall, the antenna positioning mechanism adds functionality and capabilities to TESS and brings it closer to meeting the mission requirements of finding exoplanets. The modification requirements were met. Increasing the sky coverage by 1.84% might allow us to find more exoplanets and learn more about the space and beyond. The cost of added mass, volume, power consumption, and monetary cost are worth the efforts to make this improvement.

6.2 Conclusions about the Piezoelectric System

6.2.1 Technical Summary of New and Lost Capability of TESS

With the piezoelectric ACS system, we gain the capability to more precisely control the attitude of TESS, which could improve our data. However, by getting rid of the reaction wheels, we lost the capability to slew.

6.2.2 Strengths and Weaknesses of New Design

The strengths of the piezoelectric system are increased precision in attitude control, lower mass, which saves money, and a smaller internal volume, which allows for more room for the stowed deployable mast.

The weaknesses of the piezoelectric ACS system include it being very brittle due to our decision to make it out of ceramic material. Another weakness is the fact that removing the reaction wheels removes TESS' ability to slew and the fact that the control sphere may saturate, requiring thrusters to desaturate them. Weaknesses of the analysis of this modification include the many assumptions we had to make in order to simplify the analysis.

6.2.3 Verdict on Piezoelectric System

Overall, the piezoelectric system meets the modification requirements, but is not a feasible modification. There is a lot still unknown about this technology and more testing is necessary before it can be used effectively. In addition, we would probably need to keep the reaction wheels in if we were to add the piezoelectric system because we need to retain the capability to slew as well as the possibility of using the wheels for desaturation of the piezoelectric spheres.

6.3 Remaining Questions and How to Resolve Them

We are still unsure about how exactly the piezoelectric system will work. It is still at a very low technology readiness level and therefore requires a lot more testing before actual implementation.
In addition, we are not sure if we would need to or be able to add the piezoelectric system while keeping the reaction wheels and thrusters already onboard TESS. A

combination of ACS systems might be better than simply replacing the current system. More analysis would be required in order to determine the best system.

6.4 Lessons Learned-What to Do Differently Next Time

What we will do differently next time is try to integrate the piezoelectric system into the spacecraft without taking out the current system, as they could be used together for the most precise and accurate pointing and stability when observing the mission sector. For example, the piezoelectric actuators could be used for attitude control while the reaction wheels desaturate them. There is so much more to learn about the piezoelectric system and a lot more analyses to perform before we are able to use them.

In addition, next time, we will try to reduce the amount of assumptions we made so that we can get more accurate results from our analyses.

References

[1] Erickson, K. et al. *10 Steps to Confirm a Planet Around Another Star*. NASA <https://solarsystem.nasa.gov/news/542/10-steps-to-confirm-a-planet-around-another-star/>.

[3] Dunbar, B. et al. *The Hubble Story*. NASA. 18 September 2018. <https://www.nasa.gov/content/the-hubble-story>.

[2] Dunbar, B. et al. *About the Hubble Space Telescope*. NASA. 18 December 2018. <https://www.nasa.gov/mission_pages/hubble/story/index.html>.

[4] *Fast Facts*. Jet Propulsion Laboratory. 23 February 2019 <http://www.spitzer.caltech.edu/mission/277-Fast-Facts>.

[5] Dunbar, B. et al. *Spacecraft and Instrument*. 3 August 2017. <https://www.nasa.gov/mission_pages/kepler/spacecraft/index.html>.

[6] Dunbar, B. et al. *Briefing Materials: NASA Retires the Kepler Space Telescope*. <https://www.nasa.gov/kepler/presskit>.

[7] *Tess Factsheet*. Northrop Grumman Corporation. 2018. <http://www.northropgrumman.com/Capabilities/ScienceEnvironmentSatellites/Documents/TESS_Factsheet.pdf>.

[8] *Science Writer's Guide*. April 2018. <https://www.nasa.gov/sites/default/files/atoms/files/tessscience writersguidedraft23.pdf>.

[9] Dunbar, B., et al. *Hubble Servicing Mission Overview*. NASA. December 2018. <https://www.nasa.gov/mission_pages/hubble/servicing/index.html>.

[10] Hunter, R. *Kepler Mission Management Update*. July 24 2012. <https://www.nasa.gov/mission_pages/kepler/news/keplerm-20122407.html>.

[11] Bansevicius, R. et. al. *SYNTHESIS OF TRAJECTORIES IN PIEZOELECTRIC ATTITUDE CONTROL DEVICES FOR NANOSATELLITES*. 11th International Conference on Vibration Problems, Z. Dimitrovová et al. (eds.), Lisbon, Portugal, 9-12 September 2013.

[12] Preumont, André. *Chapter 4: Piezoelectric Beam, Plate and Truss*. *Vibration Control of Active Structures : An Introduction* (2018). Springer International Publishing AG 2018. pp.67-70

[13] Bakanauskas V. et al. *Piezoelectric Devices for Attitude Control of Pico and Nano-Satellites*. Space Economy in the MultiPolar World, 2013, Vilnius.

[14] Honeywell. *HR-04 Reaction Wheel System*. 2018.

[15] Spaceflight 101. *TESS Spacecraft Platform*. <http://spaceflight101.com/tess/tess-spacecraft/>.

[16] Northrop Grumman. *TESS Discovering Exoplanets Orbiting Nearby Stars*. Northrop Grumman. 2018. <http://www.northropgrumman.com/Capabilities/ScienceEnvironmentSatellites/Documents/TESS_Factsheet.pdf>.
[17] Bradford. Coarse Sun Sensor. Bradford. January 2017. <http://bradford-space.com/assets/pdf/be_datasheet_css_2017jan.pdf>.
[18] Spacecraft. NASA. <https://solarsystem.nasa.gov/missions/dawn/technology/spacecraft/>.
[19] Engler, T. et al. Vibration Lab. NASA. February 2019. <https://kscpartnerships.ksc.nasa.gov/Partnering-Opportunities/Capabilities-and-Testing/Testing-and-Labs/Materials-Science/Vibration%20Lab>.
[20] Engler, T. et al. Prototype Development Laboratory. NASA. February 2019. <https://kscpartnerships.ksc.nasa.gov/Partnering-Opportunities/Capabilities-and-Testing/Testing-and-Labs/Materials-Science/Prototype-Development-Lab>.
[21] Vernier R. NASA GODDARD SPACE FLIGHT CENTER: THE ACOUSTIC TEST FACILITY. NASA. <https://scap.hq.nasa.gov/docs/SCAP_ACOUSTIC_112508_508.pdf>.
[22] Ramirez R. Shuttle Radar Topography Mission The Mission to Map the World. NASA. March 2019. <https://www2.jpl.nasa.gov/srtm/mast.html>.
[23] Wassmer W. The Materials Used in Artificial Satellites and Space Structures. AZO Materials. May 2015. <https://www.azom.com/article.aspx?ArticleID=12034>.
[24] Elhajjar, R., La Saponara, V., Muliana, A. *Chapter 4: Active Fiber Composites: Modeling, Fabrication, and Characterization*. *Smart Composites: Mechanics and Design*. CRC Press. 2014. pp. 99-127.
[25] MatWeb Material Property Data. Carpenter Invar 36 Alloy, Cold Drawn Bars. <http://www.matweb.com/search/datasheettext.aspx?matguid=b6fb00b235f0442da4d31a0cd04671c9>.
[26] MatWeb Material Property Data. Steels, General Properties. <http://www.matweb.com/search/datasheet.aspx?matguid=10e1c14130cd4ed6ae64b85723be53af&n=1>.
[27] Chromel Electrical Resistance. ConceptAlloys. <https://conceptalloys.com/electrical-resistance-alloys/>.
[28] MatWeb Material Property Data. Tungsten. <http://www.matweb.com/search/DataSheet.aspx?MatGUID=41e0851d2f3c417ba69ea0188fa570e3&ckck=1>.
[29] Center for Astrophysics. Harvard and Smithsonian. <https://www.cfa.harvard.edu/facilities/Ground-Based-Telescopes>.

[30] Dunbar B. James Webb Telescope Overview. September 2018. <https://www.nasa.gov/mission_pages/webb/about/index.html>.
[31] Kruk J. W FIRST Wide Field Infrared Survey Telescope. NASA. <https://wfirst.gsfc.nasa.gov/>.
[32] Canister Astromast. Northrop Grumman. <http://www.northropgrumman.com/BusinessVentures/AstroAerospace/Products/Documents/pageDocs/DS-303-CannisterAstroMast.pdf>.
[33] Belvin W. Keith. Et al. *Advanced Deployable Structural System for Small Satellites*. <https://ntrs.nasa.gov/archive/nasa/casi.ntrs.nasa.gov/20170003919.pdf>.
[34] Fortescue, P. et al. *Spacecraft Systems Engineering*. Fourth Edition. Wiley. 2011. p. 257.
[35] Meriam, J. et al. *Engineering Mechanics: Dynamics*. Eighth Edition. Wiley. 2015. pp. 627-633, 667-680.
[36] Meggit A/S. *Ferroperm™ Piezoelectric: Pz26 (Navy I) Hard relaxor type PZT*. March 2017. <https://www.meggittferroperm.com/wp-content/uploads/2017/10/Datasheet-hard-pz26.pdf>.
[37] Kamath A. and Hodgson B., *TESS_Sim.m*. MATLAB code used for simulations. <https://github.com/abhinavkamath/TESS/blob/master/TESS_Sim.m>.